JCI insight

Aiolos promotes CXCR3 expression on T_H1 cells via positive regulation of IFNγ/STAT1 signaling

Melissa R. Leonard, … , Jacob S. Yount, Kenneth J. Oestreich

JCI Insight. 2024. https://doi.org/10.1172/jci.insight.180287.

Research In-Press Preview Immunology Infectious disease

Graphical abstract

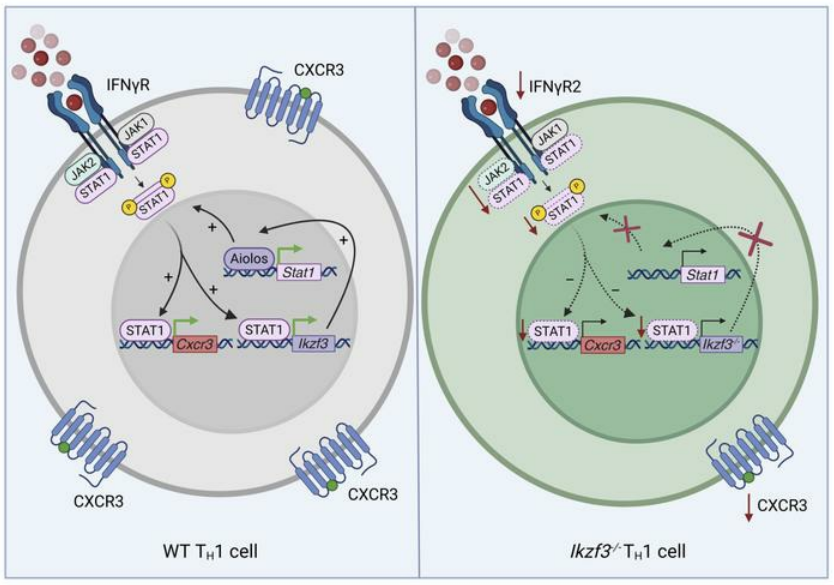

Find the latest version:

https://jci.me/180287/pdf

Title: Aiolos promotes CXCR3 expression on T_H1 cells via positive regulation of IFNγ/STAT1 signaling

Authors: Melissa R. Leonard[1,2], Devin M. Jones[1,3†], Kaitlin A. Read[1,3‡], Srijana Pokhrel[1], Jasmine A. Tuazon[1,3,4], Robert T. Warren[1], Jacob S. Yount[1,5], and Kenneth J. Oestreich[1,5,6*]

Affiliations:

[1] Department of Microbial Infection and Immunity, The Ohio State University College of Medicine and Wexner Medical Center, Columbus, OH, USA.

[2] Combined Anatomic Pathology Residency/PhD Program, The Ohio State University College of Veterinary Medicine, Columbus, OH, USA.

[3] Biomedical Sciences Graduate Program, The Ohio State University College of Medicine, Columbus, OH, USA.

[4] Medical Scientist Training Program, The Ohio State University College of Medicine, Columbus, OH, USA.

[5] Infectious Diseases Institute, The Ohio State University College of Medicine and Wexner Medical Center, Columbus, OH, USA.

[6] Pelotonia Institute for Immuno-Oncology, The Ohio State University Comprehensive Cancer Center, Columbus, OH, USA.

Present Affiliations:

[†] Discovery Immunology, Merck & Co., Inc., Cambridge, MA, USA.

[‡] Department of Microbiology, Center for Cellular Immunotherapies, University of Pennsylvania, Philadelphia, PA, USA.

* Correspondence should be addressed to K.J.O: 798 Biomedical Research Tower, 460 W. 12th Avenue, Columbus, OH 43210, USA; Email: Ken.Oestreich@osumc.edu; Phone: 614-685-3549.

Conflict-of-interest statement

The authors have declared that no conflict of interest exists.

Abstract: $CD4^+$ T helper 1 (T_H1) cells coordinate adaptive immune responses to intracellular pathogens, including viruses. Key to this function is the ability of T_H1 cells to migrate within secondary lymphoid tissues, as well as to sites of inflammation, which relies on signals received through the chemokine receptor CXCR3. CXCR3 expression is driven by the T_H1 lineage-defining transcription factor T-bet, and the cytokine-responsive Signal Transducer and Activator of Transcription (STAT) family members STAT1 and STAT4. Here, we identify the Ikaros zinc finger (IkZF) transcription factor Aiolos (*Ikzf3*) as an additional positive regulator of CXCR3 both in vitro and in vivo using a murine model of influenza virus infection. Mechanistically, we find that Aiolos-deficient $CD4^+$ T cells exhibit decreased expression of key components of the IFNγ/STAT1 signaling pathway, including JAK2 and STAT1. Consequently, Aiolos deficiency results in decreased levels of STAT1 tyrosine phosphorylation and reduced STAT1 enrichment at the *Cxcr3* promoter. We further find that Aiolos and STAT1 form a positive feedback loop via reciprocal regulation of each other downstream of IFNγ signaling. Collectively, our study demonstrates that Aiolos promotes CXCR3 expression on T_H1 cells by propagating the IFNγ/STAT1 cytokine signaling pathway.

Introduction

During adaptive immune responses to infection, naïve $CD4^+$ T cells differentiate into T "helper" subsets with distinct effector functions. T helper 1 (T_H1) cells represent one such subset that produces interferon gamma (IFNγ) and directs immune responses against intracellular pathogens. Differentiation of effector subsets is initiated when antigen-presenting cells (APCs) deliver cognate antigen to the T cell receptor (TCR) expressed on the surface of a naïve $CD4^+$ T cell. Additional signals received in the form of co-stimulatory molecules and environmental cytokines further propagate T cell activation and differentiation into specific subsets (1-5). As part of this process, signaling through cytokine receptors leads to activation of Janus kinases (JAKs) and ensuing tyrosine phosphorylation of STAT factors, which then dimerize, translocate to the nucleus, and bind to target genes (6-9). For example, IFNγ signaling via STAT1 and IL-12 signaling via STAT4 both stimulate the expression of T-bet (*Tbx21*), the lineage-defining transcription factor for the T_H1 gene program (10-12). In turn, T-bet promotes IFNγ production via direct transcriptional activation of the *Ifng* gene, thus, creating a positive feedback loop that drives T_H1 differentiation (13-15).

More recently, Ikaros Zinc Finger (IkZF) transcription factors have been implicated in the regulation of $CD4^+$ T cell programming events (16, 17). IkZF factors contain conserved N-terminal zinc finger (ZF) domains that mediate DNA-binding specificity as well as C-terminal protein-interaction domains that enable IkZF dimerization and recruitment of co-regulators, such as chromatin remodeling complexes (16-22). The importance of IkZF factors to immune cell function is underscored by studies in humans that have described missense mutations in the IkZF family member Aiolos (*Ikzf3*) that result in immunodeficiency. These changes have been associated with abnormalities in B and T cell differentiation, increased susceptibility to infectious diseases, and elevated risk for certain types of hematological malignancies (23-26). One study specifically identified a heterozygous Aiolos mutation associated with impaired T helper cell polarization, which led to reduced numbers of T follicular helper (T_{FH}) and T_H1 cells in affected patients (25).

IkZF factors have also emerged as key regulators of cytokine signaling pathways (18). Previous work from our lab identified a transcription factor complex comprised of Aiolos and STAT3 that promoted T_{FH} cell programming (18). Similarly, we established that a second IkZF/STAT factor complex comprised of Eos (*Ikzf4*) and STAT5 drives T_H2 differentiation by inducing expression of IL-4 and IL-2 cytokine receptors (27). Further, we demonstrated that Aiolos modulates IL-2 responsiveness via repression of the IL-2Rα (CD25) and IL-2Rβ (CD122) subunits, both promoting T_{FH} differentiation and suppressing cytotoxic programming of $CD4^+$ T cells (28). Beyond our findings, others have found that Aiolos regulates cytokine production, including direct silencing of the *Il2* locus in T_H17 cells (29). These collective findings suggest that a complex interplay exists between IkZF factors, cytokine signaling pathways, and T helper cell programming events, much of which remains enigmatic.

Like cytokines, chemokines signal through specific receptors, and serve as integral mediators of both $CD4^+$ T cell differentiation and migration (30-32). The chemokine receptor CXCR3 is a G protein-coupled receptor that is highly expressed on the surface of T_H1 cells (33, 34). CXCR3 responds to three interferon-inducible ligands (CXCL9, CXCL10, and CXCL11) and directs T_H1 cells to sites of inflammation (33, 35, 36). Although T_H1 cell responses are beneficial during infection, their activities are typically tightly controlled to prevent destruction of healthy tissue. To this end, aberrant activities of T_H1 cells have been implicated in autoimmunity, and therapeutically targeting CXCR3 appears to have disease-specific advantages (35, 37-43). As such, obtaining a better understanding of the transcriptional mechanisms regulating CXCR3 expression may provide additional insight for the development of novel therapeutics.

Here, we identify Aiolos as a positive regulator of CXCR3 expression in both in vitro-generated T_H1 cells and those that arise in response to murine influenza virus infection. Mechanistically, we find that Aiolos-deficient $CD4^+$ T cells have reduced expression of components of the IFNγ/STAT1 signaling pathway, which results in decreased STAT1 activation and enrichment at the *Cxcr3* promoter. We further find that *Stat1* is a direct Aiolos target gene,

with Aiolos both modulating chromatin accessibility at, and driving activity of, the *Stat1* promoter. Moreover, we demonstrate that Aiolos expression itself is dependent upon IFNγ signaling and that STAT1 directly binds the *Ikzf3* promoter. Collectively, our findings reveal that Aiolos promotes CXCR3 expression on T_H1 cells by propagating IFNγ/STAT1 signaling via a positive feedback loop with STAT1.

Results

CXCR3 expression is reduced on Aiolos-deficient CD4$^+$ T_H1 cells.

We previously reported that Aiolos functions as a repressor of CD4$^+$ T cell cytotoxic programming via suppression of IL-2/STAT5 signaling (28). In line with these findings, RNA-seq analysis of wild-type (WT) versus Aiolos-deficient (*Ikzf3*$^{-/-}$) T_H1 cells revealed increased expression of many STAT5 target genes associated with cytotoxic function, including *Gzmb*, *Prf1, Ifng*, and *Prdm1* (Figure 1A). In contrast, expression of *Cxcr3* (encoding CXCR3), a chemokine receptor that guides migration of both T_H1 cells and CD4$^+$ cytotoxic T lymphocytes (CD4-CTLs), was reduced in the absence of Aiolos (Figure 1A). Consistent with the RNA-seq data, transcript and flow cytometric analyses of in vitro-generated *Ikzf3*$^{-/-}$ T_H1 cells revealed significant decreases in both CXCR3 transcript and cell surface expression compared to WT after 3 days of differentiation (Figure 1, B-D). In accordance with previous reports describing the inhibition of CXCR3 expression with persistent TCR stimulation, the reduction in cell surface expression of CXCR3 on *Ikzf3*$^{-/-}$ T_H1 cells was further enhanced after cells were removed from stimulation with α-CD3 and α-CD28 antibodies and cultured for an additional 48 hours (Figure 1, B, E, F) (44). These findings suggested that CXCR3 expression may be regulated by an Aiolos-dependent mechanism.

We next examined the impact of Aiolos deficiency on CXCR3 expression in vivo using a murine model of influenza A virus (IAV) infection (45). WT and *Ikzf3*$^{-/-}$ mice were intranasally infected with a sublethal dose of IAV strain A/PR/8/34 (H1N1, termed “PR8”), and nucleoprotein (NP)-specific CD4$^+$ T cells of the draining, mediastinal lymph node (mLN) and lungs were assessed at 8 days post-infection (Figure 2A). There was no significant difference in the numbers of NP-specific CD4$^+$ T cells in the mLN between WT and *Ikzf3*$^{-/-}$ mice (Supplemental Figure 1A). Further analyses of the NP-specific population revealed a significant decrease in CXCR3 surface expression in the absence of Aiolos (Figure 2, B and C). In contrast to the mLN, *Ikzf3*$^{-/-}$ mice had a significant reduction in NP-specific CD4$^+$ T cells in the lungs compared to WT (Supplemental

Figure 1B). These findings are in agreement with previous reports identifying CXCR3 as an essential chemokine receptor for antigen-specific effector T cell recruitment to the lungs (46, 47). The numbers of bulk $CD4^+$ T cells in the mLN were quantified and again revealed no significant difference between WT and *Ikzf3*$^{-/-}$ mice (Supplemental Figure 1C). However, in the lungs, we observed a significant reduction in the number of bulk $CD4^+$ T cells in *Ikzf3*$^{-/-}$ mice compared to WT, though not to the extent observed with NP-specific cells (Supplemental Figure 1D). Collectively, these data suggest that migration of $CD4^+$ T cells is disrupted in Aiolos-deficient mice during pulmonary infection.

T-bet is a known positive regulator of CXCR3 expression (48-51). Thus, we next examined T-bet expression to determine whether differences in this transcriptional regulator may explain the decrease in CXCR3 expression. However, we observed no significant difference in T-bet expression between NP-specific WT and *Ikzf3*$^{-/-}$ cells, suggesting that Aiolos-dependent regulation of CXCR3 expression may occur through a T-bet-independent mechanism (Supplemental Figure 2A).

Finally, we examined CXCR3 surface expression on bulk $CD4^+$ naïve, central memory, and effector T cell populations from the spleen to determine whether the decrease in CXCR3 expression was limited to distinct $CD4^+$ T cell subsets. As expected, naïve $CD4^+$ T cells from both WT and *Ikzf3*$^{-/-}$ mice did not express CXCR3 (Supplemental Figure 2B). However, both central memory and effector $CD4^+$ T cells from *Ikzf3*$^{-/-}$ mice displayed significantly reduced CXCR3 expression compared to their WT counterparts, with a greater reduction present on effector $CD4^+$ T cells (Supplemental Figure 2, C and D). Overall, our findings in NP-specific and bulk $CD4^+$ T cells suggest that Aiolos regulates CXCR3 expression in vivo.

CXCR3 expression is reduced on Aiolos-deficient $CD4^+$ T cells in a cell-intrinsic manner.

To assess whether the impact of Aiolos on CXCR3 expression was $CD4^+$ T cell-intrinsic, we crossed WT and *Ikzf3*$^{-/-}$ mice onto the OT-II background, which expresses a transgenic TCR

specific for the ovalbumin 323-339 peptide (OVA). We then adoptively transferred naïve CD45.2$^+$ CD4$^+$ T cells from either WT-OT-II or *Ikzf3*$^{-/-}$-OT-II mice into WT CD45.1$^+$ recipients. Recipient mice were subsequently infected with $OVA_{323-339}$-expressing PR8 (PR8-OVA) 24 hours post-transfer and antigen-specific CD45.2$^+$ donor cells from the mLN were analyzed via flow cytometry at 8 days post-infection (Figure 3A). Consistent with our findings in Aiolos-deficient mice, we observed a significant decrease in CXCR3 expression on donor CD45.2$^+$ *Ikzf3*$^{-/-}$ cells compared to WT (Figure 3, B and C). We also noted a slight downregulation in T-bet expression in *Ikzf3*$^{-/-}$ compared to WT CD45.2$^+$ donor cells (Supplemental Figure 3A). However, the fold reduction in CXCR3 expression was greater than that of T-bet. Collectively, these findings demonstrate that the impact of Aiolos on CXCR3 expression occurs in a CD4$^+$ T cell-intrinsic manner.

We next quantified the numbers of antigen-specific CD45.2$^+$ donor cells in the mLN and lungs of recipient mice. In the mLN, there was no significant difference between the number of WT-OT-II and *Ikzf3*$^{-/-}$-OT-II cells, and only a slight but significant decrease in the frequency of Aiolos-deficient cells (Supplemental Figure 3B). In contrast to our findings in germline knockout animals, there was no significant difference in cell numbers or percentages between donor WT-OT-II and *Ikzf3*$^{-/-}$-OT-II cells in the lungs (Supplemental Figure 3C). These data indicate that the migration of donor T cells to the lungs is not impaired when cells are intravenously injected into recipient mice, despite the observed reduction in CXCR3 expression. Thus, while Aiolos regulates CXCR3 expression in CD4$^+$ T cell-intrinsic manner, alterations in CXCR3 expression do not ultimately have a cell-intrinsic effect on migration of adoptively transferred cells to the lungs.

To determine a potential explanation, we analyzed published RNA-seq data (GSE203065) from WT and *Ikzf3*$^{-/-}$ T_H1 cells. As with *Cxcr3*, various adhesion molecules and integrin subunits were downregulated in the absence of Aiolos. However, several other chemokine receptors known to promote T_H1 cell migration (i.e. *Ccr5*, *Cxcr6*) were upregulated in Aiolos-deficient cells relative to WT (Supplemental Figure 3D). Hence, the impact of Aiolos on migratory programming

appears to be multilayered with alterations to other migratory receptors potentially compensating for the loss of CXCR3 in the adoptive transfer setting.

Aiolos deficiency alters expression of components of the IFNγ/STAT1 and IL-12/STAT4 pathways.

We next sought to identify the mechanism(s) by which Aiolos may regulate CXCR3 expression in T_H1 cells. In addition to T-bet, CXCR3 expression is regulated by STAT1 and STAT4 (44, 52-54). Comparison of publicly available Chromatin Immunoprecipitation sequencing (ChIP-seq) data for STAT1 (GSM994528), STAT4 (GSM550303), and T-bet (GSM836124) revealed enrichment of these factors at the promoter and 3' enhancer regions of the *Cxcr3* locus (Figure 4A) (48-51, 55-58). Analysis of published RNA-seq data (GSE203065) from WT and *Ikzf3*$^{-/-}$ T_H1 cells showed that the expression of key components of the IFNγ/STAT1 and IL-12/STAT4 signaling pathways was altered in the absence of Aiolos. Specifically, *Jak2* and *Stat1* were downregulated in *Ikzf3*$^{-/-}$ compared to WT T_H1 cells (Figure 4B) (28). Notably, *Jak2*, which is shared between the IFNγ and IL-12 pathways, was the only Janus kinase that was significantly downregulated in *Ikzf3*$^{-/-}$ T_H1 cells (findings available in Source Data). Further, genes encoding the IFNγ and IL-12 cytokine receptor subunits, *Ifngr2* and *Il12rb1*, also displayed slight decreases in the absence of Aiolos (Figure 4B). Given that many of the altered genes encode proteins involved in IFNγ/STAT1 and IL-12/STAT4 signaling, we hypothesized that Aiolos may regulate CXCR3 via impacts on these pathways (Figure 4C).

IFNγ/STAT1 signaling, but not IL-12/STAT4, is diminished in the absence of Aiolos.

We next assessed the impact(s) of Aiolos on IFNγ/STAT1 and IL-12/STAT4 signaling with WT and *Ikzf3*$^{-/-}$ $CD4^+$ T cells cultured under T_H1 conditions. Previous work from our lab has established that Aiolos-deficient T_H1 cells have enhanced IFNγ production upon stimulation (28). To control for this, as well as any other cytokines produced by $CD4^+$ T cells in culture, cells were removed

from stimulation on day 3 of differentiation and cultured for an additional 2 days with IL-12 before being harvested for analysis (Figure 5A). Transcript analysis of IL-12-treated cells revealed significant decreases in *Cxcr3*, *Stat1*, *Jak2*, and *Ifngr2* in *Ikzf3*$^{-/-}$ relative to WT T_H1 cells. In contrast, transcript levels for *Stat4* and *Il12rb2* were significantly increased in *Ikzf3*$^{-/-}$ T_H1 cells compared to WT (Figure 5B and Supplemental Figure 4A). No significant difference in transcript for *Tbx21* was observed between groups (Figure 5B). Immunoblot analyses similarly revealed significant reductions in total JAK2 and STAT1 protein in the absence of Aiolos (Figure 5, C and D). In contrast, tyrosine-phosphorylated STAT4 (pY-STAT4) and total STAT4 protein levels were significantly elevated in the absence of Aiolos (Figure 5C), demonstrating that the STAT4 pathway is not functionally inhibited by Aiolos deficiency when cells are treated with IL-12.

To more directly assess the impact of Aiolos-deficiency on the IFNγ/STAT1 signaling pathway, we cultured WT and *Ikzf3*$^{-/-}$ $CD4^+$ T cells under T_H1 conditions for 3 days, and then added IFNγ, rather than IL-12, for an additional 48 hours in the absence of stimulation (Figure 6A). Again, *Ikzf3*$^{-/-}$ T_H1 cells had significantly reduced expression of *Cxcr3*, *Stat1*, *Jak2*, and *Ifngr2* compared to WT, whereas *Stat4* and *Il12rb2* transcripts were consistently increased (Figure 6B and Supplemental Figure 4B). In contrast to IL-12-treated cells, we also found that *Tbx21* expression was significantly decreased in Aiolos-deficient cells, suggesting that IFNγ/STAT1 signaling is unable to compensate for the lack of IL-12/STAT4-dependent activation of T-bet expression in the absence of Aiolos (Figure 6B) (54).

Flow cytometry analysis similarly revealed a significant decrease in CXCR3 surface expression on *Ikzf3*$^{-/-}$ cells compared to WT (Figure 6C). Immunoblot analyses showed significant reductions in total JAK2, tyrosine-phosphorylated STAT1 (pY-STAT1), and total STAT1 protein in the absence of Aiolos (Figure 6D). However, total STAT4 protein remained significantly elevated in *Ikzf3*$^{-/-}$ T_H1 cells (Supplemental Figure 4C). Thus, across IL-12 and IFNγ simulation conditions, only JAK2 and STAT1 correlated with the reduced CXCR3 expression observed in the absence of Aiolos.

We next examined publicly available STAT1 ChIP-seq data (GSM994528) to identify STAT1-binding regulatory regions at the *Cxcr3* locus that may be impacted by Aiolos-deficiency and performed ChIP analysis of IFNγ-treated WT versus *Ikzf3*$^{-/-}$ T_H1 cells (Figure 6E) (56). Coincident with the loss of STAT1 expression, we observed a significant decrease in STAT1 enrichment at the *Cxcr3* promoter and a trending decrease in STAT1 enrichment at the *Cxcr3* 3' enhancer region (p = 0.0697) in the absence of Aiolos (Figure 6F). These collective data demonstrate that the IFNγ/STAT1 pathway is compromised by Aiolos deficiency and that Aiolos functions to positively regulate CXCR3 expression via STAT1.

IFNγ/STAT1 signaling induces Aiolos expression.

We next wanted to examine how directly inhibiting IFNγ signaling may impact the relationship between Aiolos, STAT1, and CXCR3. We cultured WT naïve $CD4^+$ T cells under T_H1 conditions for 3 days with the addition of an IFNγ-neutralizing antibody to inhibit autocrine IFNγ signals (Figure 7A). Neutralizing IFNγ led to significant reductions in *Cxcr3*, *Stat1*, and *Jak2* expression (Figure 7B) (44, 52). Flow cytometric and immunoblot analyses similarly revealed significant reductions in CXCR3, total JAK2, total STAT1, and pY-STAT1 protein levels when IFNγ was neutralized (Figure 7, C and D). Notably, Aiolos expression was also significantly decreased with IFNγ neutralization, suggesting a possible positive feedback loop between Aiolos and IFNγ/STAT1 (Figure 7E).

Aiolos and STAT1 are enriched at the *Stat1* and *Ikzf3* promoters, respectively.

Given the positive correlation between Aiolos and STAT1 expression, we performed an in silico analysis for the core IkZF factor DNA-binding motif "GGGAA" at the *Stat1* locus and found several predicted binding sites at the promoter region. Subsequent examination of publicly available Aiolos ChIP-seq data (GSM5106065) revealed a region of Aiolos enrichment at the *Stat1* promoter (Figure 8A) (23). These findings suggested that *Stat1* could be a direct target gene of

Aiolos in T_H1 cells. Since IkZF factors are known regulators of chromatin structure, we examined previously published Assay for Transposase-Accessible Chromatin (ATAC)-seq data (GSE203064) from WT and *Ikzf3*$^{-/-}$ cells cultured under T_H1 conditions. Indeed, in the absence of Aiolos, we observed a significant decrease in chromatin accessibility at the *Stat1* promoter (Figure 8A) (28).

To test whether Aiolos could regulate *Stat1* promoter activity, we created a *Stat1* promoter-reporter construct encompassing the Aiolos-enriched region. We then overexpressed with WT Aiolos or an Aiolos DNA-binding mutant (Aiolos^{DBM}) containing point mutations in the first two N-terminal zinc finger domains, rendering this domain non-functional (Figure 8B) (18). We observed a significant increase in *Stat1* promoter activity upon overexpression of WT Aiolos, and this induction was lost upon overexpression of Aiolos^{DBM} (Figure 8C). These findings indicate that Aiolos is capable of inducing *Stat1* promoter activity and that the DNA-binding domain is required.

Lastly, to determine whether STAT1 may reciprocally regulate Aiolos expression, we examined publicly available ChIP-seq data for STAT1 (GSM994528) and previously published ATAC-seq data (GSE203064) from WT T_H1 cells. Indeed, we identified a potential region of STAT1 enrichment at the *Ikzf3* promoter, which correlated with a region of accessible chromatin in T_H1 cells (Figure 8D) (28, 56). Further, ChIP analysis of IFNγ-treated WT T_H1 cells revealed that STAT1 was enriched at the *Ikzf3* promoter relative to an upstream control region (Figure 8E). Collectively, these data support the existence of a positive feedback loop between Aiolos and STAT1 through which IFNγ/STAT1 signaling and CXCR3 expression are regulated.

Discussion

Aiolos has long been implicated in lymphoid cell development (16, 19-22). More recently, Aiolos has emerged as a regulator of cytokine signaling pathways and effector programs in innate and adaptive lymphocytes (17, 18, 27). Here, we have identified Aiolos as a positive regulator of IFNγ/STAT1 signaling and a driver of CXCR3 expression in T_H1 cells. Our observations are consistent with findings from earlier studies indicating that IFNγ and STAT1 are critical for induction of CXCR3 on $CD4^+$ T cells (44, 52). The work presented here expands upon those findings by uncovering Aiolos as a positive transcriptional regulator of STAT1, and that IFNγ/STAT1 subsequently promotes Aiolos expression through a feed-forward amplification loop.

In contrast to STAT1, we found that expression of both tyrosine-phosphorylated and bulk STAT4 protein was elevated in Aiolos-deficient cells. Relatedly, others have reported an inverse correlation between activation of STAT4 and overall levels of STAT1 in Natural Killer (NK) cells (59). We also observed that Aiolos deficiency resulted in reduced expression of JAK2, a kinase of the IL-12/STAT4 signaling pathway. One explanation for this apparent contradiction may be that alterations in expression of other cytokine signaling pathway components offsets reduced JAK2 levels. For example, we have previously shown that Aiolos deficiency allows for enhanced IL-2 sensitivity, and it has been established that IL-2 induces expression of *Il12rb2* (28, 60). Previous work has demonstrated that TYK2, another non-receptor tyrosine kinase involved in IL-12/STAT4 signaling is critical for STAT4-mediated IFNγ expression (61). Future studies are needed to determine whether TYK2 activation may contribute to sustained IL-12/STAT4 signaling despite the loss of JAK2 in the absence of Aiolos.

We found that adoptively transferred Aiolos-deficient cells do not exhibit altered migration to the lungs, despite reduced CXCR3 expression. In addition to CXCR3, the chemokine receptor CCR5 is also known to enable T_H1 cell migration, and previous work has demonstrated that IL-12/STAT4 signaling selectively upregulates CCR5 (44, 62, 63). Indeed, we find elevated *Ccr5* transcript in Aiolos-deficient cells suggesting that it may compensate for reduced CXCR3

expression. Finally, given that both STAT1 and STAT4 positively impact T-bet expression, the counter-regulatory nature of Aiolos on IFNγ/STAT1 and IL-12/STAT4 signaling may help to explain the inconsistent alterations in T-bet expression that we observed in the absence of Aiolos. Our finding that CXCR3 and T-bet expression do not consistently correlate further supports the conclusion that another Aiolos-dependent factor (i.e. STAT1) is responsible for regulating CXCR3 expression. Indeed, STAT1 has been shown to control T_H1 trafficking to the lung through a T-bet-independent mechanism (64).

IFNγ/STAT1 signaling operates across multiple cell types suggesting that the regulatory mechanisms established here may extend to additional Aiolos-expressing immune cells, such as Innate Lymphoid Cells (ILCs), $CD8^+$ T cells, and B cells (16, 65-73). It is also possible that Aiolos could impact other STAT1-driven cytokine pathways (i.e. IFNα/β/λ, IL-27, IL-6) (74-76). For example, a recent study indicated that Aiolos promotes the proliferation and survival of HIV-1 infected cells, which was associated with the upregulation of genes involved in T cell migration and type I IFN responses (77). Work by others in $CD8^+$ T cells has shown that reduced levels of STAT1, maintained by STAT4, are required for overcoming the anti-proliferative effects of type I IFN during viral infection (59). This is just one example suggesting that Aiolos-dependent alterations in STAT1 expression could impact other signaling pathways.

Studies in humans have described *IKZF3* missense mutations that compromise the DNA-binding domain and result in primary immunodeficiency and inborn errors of immunity (23-26). Two such mutations, termed G159R and N160S, have been reported in humans and are associated with increased susceptibility to infections and dysregulated immune responses. The *IKZF3* G159R mutation has been associated with B cell deficiency, B cell malignancy, and abnormal T cell differentiation (23). Similarly, the *IKZF3* N160S mutation has been shown to affect both B and T cell populations, leading to increased susceptibility to infection. With regard to T cells, the *IKZF3* N160S mutation results in decreased T_{FH}, T_H1, and memory T cell populations (25). Thus, our finding that Aiolos regulates IFNγ/STAT1 signaling may provide at least some

mechanistic explanation for these observed disruptions in humans. Overall, these findings underscore the clinical consequences arising from genetic defects in Aiolos function, notably including compromised T_H1 responses.

While chemokine receptor expression is normally restricted to lymphocyte populations, many cancers are known to aberrantly express these receptors and consequently acquire migratory (metastatic) abilities, a phenomenon termed 'lymphocyte mimicry' (78, 79). Aiolos has been linked to metastatic lung cancer through the induction of such pathways, including expression of CXCR4 (80-82). Of note, previous work from our lab has demonstrated that Aiolos promotes CXCR5 expression in T_{FH} cells, which enables their migration into B cell follicles (18, 28). More recent work has demonstrated that T and B cells homozygous for an Aiolos missense mutation exhibit impaired homing into lymph nodes primarily due to low CD62L expression (83). These studies, alongside our observation of disrupted CXCR3 expression and altered transcript levels for multiple cell adhesion molecules, integrin subunits, and chemokine receptors in Aiolos-deficient T_H1 cells, suggest that Aiolos drives a larger immune cell migratory program, which ultimately requires further investigation.

Finally, JAK-STAT signaling pathways have long been the target of different therapeutics due to demonstrated roles in autoimmune diseases and hematological malignancies (6-9, 84-88). Similarly, Aiolos has been targeted therapeutically with lenalidomide, an immunomodulatory drug used to treat multiple myeloma and various lymphomas (89-92). Lenalidomide has also been shown to enhance the cytotoxic activity of CAR T cells against solid tumors, which is consistent with previous work showing that Aiolos suppresses T cell cytotoxic function (28, 93-95). However, given the current study, it is reasonable to postulate that loss of Aiolos could also result in altered lymphoid migratory patterns during immune responses to infection or cancer, which would be consistent with findings in human patients harboring Aiolos missense mutations (23-26). Hence, therapeutics that specifically target Aiolos may have disease-specific advantages and disadvantages, presenting a potential paradox. Ultimately, future studies will be required to

388 determine the full extent of effects of Aiolos on immune cell programming, including its impact on
389 STAT1-dependent signaling pathways**.**
390
391 **Methods**
392 **Sex as a biological variable**
393 Germline knockout influenza virus infection studies and all in vitro experiments utilized both male
394 and female mice to avoid unintentional sex bias. Similar findings are reported for both sexes. For
395 adoptive transfer studies, only male donor and recipient mice were utilized due to the Y-linked
396 nature of the OT-II transgene.
397
398 **Mouse strains**
399 Wild-type CD45.1 (JAX stock #002014) and CD45.2 C57BL/6J (JAX stock #000664) mice were
400 originally obtained from the Jackson Laboratory. Aiolos-deficient (*Ikzf3*$^{-/-}$) mice were originally
401 obtained from Riken BRC and were backcrossed onto the CD45.2 C57BL/6J Jackson background
402 for more than 10 generations. OT-II mice (JAX stock #004194), with the transgene located on the
403 Y-chromosome, were originally generated by the Carbone laboratory (96) and were a generous
404 gift from Dr. Haitao Wen (The Ohio State University, Columbus, OH). For adoptive transfer
405 studies, *Ikzf3*$^{-/-}$ mice were crossed to OT-II mice to generate *Ikzf3*$^{-/-}$-OT-II mice. For all experiments
406 and replicates, individual mice were age- and sex-matched.
407
408 **CD4$^+$ T cell isolation and culture**
409 Naïve CD4$^+$ T cells were isolated from the spleens and lymph nodes of 5-8-week-old mice using
410 the BioLegend Mojo Sort naïve CD4$^+$ T cell isolation kit according to the manufacturer's
411 recommendations. For in vitro polarization of T_H1 cell populations, naïve CD4$^+$ T cells were plated
412 at a density of 300,000 cells/well in complete IMDM (IMDM [Life Technologies], 10% FBS
413 [26140079, Life Technologies], 1% penicillin/streptomycin [Life Technologies], and 0.05% (50 μM)

2-mercaptoethanol [Sigma-Aldrich]). Plates were coated with anti-CD3 (clone 145-2C11; 5 µg/mL; BD Biosciences) and anti-CD28 (clone 37.51; 2 µg/mL; BD Biosciences) overnight and washed twice with PBS prior to the addition of cells in complete IMDM. Upon plating, cells were cultured in the presence of IL-4 neutralizing antibody (clone 11B11; 5 µg/mL; BioLegend) and the T_H1-polarizing cytokine rmIL-12 (5 ng/mL; R&D) for 72 hours prior to analysis or expansion. For experiments in which IFNγ was neutralized, cells were also cultured in the presence of α-IFNγ antibody (clone XMG1.2; 10 µg/mL; BioLegend) for 72 hours. For expansion of cells on day 3 into resting conditions, cells were plated at 500,000 cells/well in complete IMDM with the addition of fresh IL-4 neutralizing antibody (clone 11B11; 5 µg/mL; BioLegend), rhIL-2 (250 U/ml; Peprotech), and either fresh rmIL-12 (5 ng/mL; R&D) or rmIFNγ (50 ng/mL; Peprotech), as noted. Cells were cultured for an additional 48 hours prior to harvesting for analysis on day 5. For experiments in which cells were cultured in the presence of rmIFNγ, fresh rmIFNγ (50 ng/ml; Peprotech) was added 1 hour prior to harvest.

RNA isolation and qRT-PCR

Total RNA was isolated from the cell populations described above using the Macherey-Nagel Nucleospin RNA Isolation kit according to the manufacturer's guidelines. cDNA was generated using the Superscript IV First Strand Synthesis System (Thermo Fisher Scientific). qRT-PCR reactions were performed using the SYBR Select Mastermix for CFX (Thermo Fisher Scientific) with 10 ng cDNA per reaction and primers for the appropriate genes (Supplemental Table 1). All qRT-PCR reactions were performed on the CFX Connect (BioRad). Data were normalized to *Rps18* and are presented as relative to the WT control sample.

RNA sequencing analysis

Published RNA-seq data (GSE203065) from WT and *Ikzf3*$^{-/-}$ T_H1 cells was analyzed as previously reported (28). Briefly, naïve $CD4^+$ T cells were cultured under T_H1-polarizing conditions for 3 days.

Total RNA was isolated using the Macherey-Nagel Nucleospin RNA Isolation kit according to the manufacturer's guidelines. Samples were provided to Azenta Life Sciences for polyA selection, library preparation, sequencing, and DESeq2 analysis (3 biological replicates per genotype from 3 independent experiments). Genes with an adjusted $p < 0.05$ were considered differentially expressed. Heatmap generation and clustering (by Euclidean distance) were performed using normalized log2 counts from DESeq2 analysis and the Morpheus software (https://software.broadinstitute.org/morpheus/). Volcano plots were generated using $-\log_{10}$(adjusted p value) and log2 fold change values from DESeq2 analysis and VolcaNoseR software (https://huygens.science.uva.nl/VolcaNoseR/) (97).

ATAC-seq analysis

Published ATAC-seq data (GSE203064) from WT and *Ikzf3*$^{-/-}$ cells cultured under T_H1 conditions was analyzed as previously described (28, 67). Briefly, 5×10^4 cells with greater than 95% viability were processed with the Illumina Nextera DNA Library Preparation Kit according to the manufacturer's instructions. Resultant sequences were trimmed and aligned to mm10 using Bowtie2. All subsequent analyses were performed using the indicated tools in Galaxy (usegalaxy.org). Samples were filtered by read quality (>30), as well as to remove duplicates and mitochondrial reads. Statistically significant peaks were identified using MACS2 callpeak. DiffBind was used to identify regions of significant differential accessibility between WT and *Ikzf3*$^{-/-}$ samples. Regions with adjusted $p < 0.05$ were considered statistically significant. CPM-normalized tracks were visualized using Integrative Genomics Viewer (IGV) versions 2.12.3 and 2.18.2.

Immunoblot analysis

Cells were harvested, counted, and lysed in 1X SDS loading dye, (50 mM Tris [pH 6.8], 100 mM DTT, 2% SDS, 0.1% bromophenol blue, 10% glycerol) and boiled for 15 minutes. Equal protein

lysate amounts were loaded based on cell counts. Lysates were separated via SDS-PAGE on 10% Bis-Tris Bolt gels (Thermo Fisher Scientific) and then transferred onto a 0.45 µm nitrocellulose membrane. Following transfer, nitrocellulose membranes were blocked with 2% non-fat dry milk in 1X TBST (10 mM Tris [pH 8.0], 150 mM NaCl, 0.05% Tween-20). The following antibodies were used to detect proteins: α-JAK2 (1:1,000; #3230, Cell Signaling Technology), α-pY-STAT4 (1:1,000; #5267, Cell Signaling Technology), α-STAT4 (1:1,000; #2653S, Cell Signaling Technology), α-pY-STAT1 (1:1,000; #9167S, Cell Signaling Technology), α-STAT1 (1:1,000; sc-417, Santa Cruz Biotechnology), α-Aiolos (1:20,000; #39293, Active Motif), α-β-actin-HRP (1:15,000; A00730, GenScript), goat α-mouse (1:5,000; 115-035-174, Jackson Immunoresearch), and mouse α-rabbit (1:5,000-1:10,000; sc-2357, Santa Cruz Biotechnology). Immunoblot bands were quantified using ImageJ as previously described (27). For each protein row, the largest band was framed, and the mean gray value was measured using the same frame across the row. Background measurements were taken with the same frame measuring the area above or below bands in the image. Pixel densities were inverted, background values were subtracted from sample and control bands, and a ratio of net protein bands to net loading control bands was calculated for protein quantification relative to the WT sample.

Influenza virus infection and tissue preparation

Influenza A virus strain A/PR/8/34 (H1N1, “PR8”) and $OVA_{323-339}$-expressing PR8 (“PR8-OVA”) were propagated in 10-day-old specific pathogen free embryonated chicken eggs (Charles River Laboratories) and titered on MDCK cells (BEI Resources, NIAID, NIH: Kidney [Canine], Working Cell Bank, cat. # NR-2628). Mice between 8-12 weeks of age were infected intranasally with 30 plaque forming units (PFU) of PR8. After 8 days, mLN, spleen, and lungs were harvested as previously described (28). For mLN and spleen, single-cell suspensions were generated in tissue processing media (IMDM + 4% FBS) by passing the tissue through a 100 µm nylon mesh strainer followed by erythrocyte lysis via a 3-minute incubation at room temperature in 0.84% NH_4Cl. For

lungs, single cell suspensions were generated by incubating whole lung tissue in HBSS (Gibco) supplemented with 1.3 mM EDTA for 30 minutes at 37°C. Following this, lungs were processed in media (RPMI + 4% FBS) supplemented with Collagenase IV using a gentleMACS Dissociator (Miltenyi Biotech) for 30 minutes according to the manufacturer's instructions. Samples were then filtered through a 40 µm nylon mesh strainer and subsequently centrifuged with a Percoll density gradient to isolate the mononuclear layer. Erythrocyte lysis was performed as previously described. For all tissues, cells were washed in FACS buffer (PBS + 4% FBS) prior to staining for flow cytometry. For adoptive transfer studies, naïve CD45.2$^+$ OT-II CD4$^+$ T cells were purified from WT-OT-II or *Ikzf3*$^{-/-}$-OT-II mice using negative selection as described above. Cells were washed and resuspended in sterile 1X PBS and transferred retro-orbitally (5×10^5 cells/animal) into WT CD45.1$^+$ recipient mice that were anesthetized with isoflurane. After 24 hours, mice were infected intranasally with 40 PFU of PR8-OVA.

Flow cytometry

For analysis of influenza nucleoprotein (NP)-specific CD4$^+$ T cells in germline *Ikzf3*$^{-/-}$ animals, cells were first incubated for at least 5 minutes at 4°C with TruStain FcX (anti-mouse CD16/32) Fc block (clone 93; 101320; BioLegend). Samples were then stained with IA^b $NP_{311-325}$ MHC class II tetramer (1:100; NIH Tetramer Core Facility) in the presence of Fc block for 1 hour at room temperature protected from light. Extracellular markers were stained in the presence of Fc block for 30 minutes at 4°C protected from light using the following antibodies: anti-CD4 (PE/Cy7; 1:300; clone GK1.5; BD Biosciences, cat. # 563933), anti-CD4 (APC; 1:300; clone GK1.5; BioLegend, cat. # 100412), anti-CXCR3 (PE; 1:300; clone CXCR3-173; BioLegend, cat. # 126505), anti-CXCR3 (BV421; 1:300; clone CXCR3-173; BioLegend, cat. # 126529), anti-CD44 (V450; 1:300; clone IM7; BD Biosciences, cat. # 560452), anti-CD44 (FITC; 1:300; clone IM7; Thermo Fisher Scientific, cat. # 553133), anti-CD62L (APC-efluor780; 1:300; clone MEL-14; Thermo Fisher Scientific, cat. # 47-0621-82), anti-CD45.1 (BV421; 1:300; clone A20; BioLegend, cat. # 110732)

anti-CD45.2 (APC; 1:300; clone 104; BioLegend, cat. # 109814). At the same time, cells were stained with Ghost viability dye (V510; 1:400; Tonbo Biociences, cat. # 13-0870-T100). Cells were then washed twice with FACS buffer prior to intracellular staining. For intracellular staining, cells were fixed and permeabilized using the eBioscience Foxp3 transcription factor staining kit (Thermo Fisher Scientific, cat. # 00-5523-00) for 30 minutes or overnight at 4°C. After fixation, samples were stained with the following antibodies in 1X eBioscience permeabilization buffer (Thermo Fisher Scientific) for 30 minutes at room temperature protected from light: anti-T-bet (PerCP-Cy5.5; 1:100; clone 4B10; BioLegend, cat. # 644806) and anti-Aiolos (AF647; 1:100; clone; S48-791; BD Biosciences, cat. # 565265). Cells were washed twice with 1X permeabilization buffer and resuspended in FACS buffer for analysis. Samples were run on a BD FACS Canto II flow cytometer and analyzed using FlowJo software (version 10.8.1). Representative gating strategies can be found in Supplemental Figures 5-7.

Promoter-reporter assay

A *Stat1* promoter-reporter construct (pGL3-*Stat1*) was generated by cloning the regulatory region of *Stat1* (positions – 479 to 0 bp) into the pGL3-Promoter vector (Promega) (Supplemental Table 2). Aiolos contains four N-terminal zinc finger (ZF) domains that mediate its DNA-binding capability. Of these four zinc fingers, ZF2 and ZF3 are required for DNA binding, whereas ZF1 and ZF4 are responsible for regulating sequence specificity (16-20). Expression vectors for WT Aiolos and an Aiolos DNA-binding mutant (Aiolos^{DBM}) were constructed as previously described (18). Briefly, two cystine residues in both ZF1 and ZF2 of Aiolos were mutated to alanine residues via site-directed mutagenesis, rendering the Aiolos DNA-binding domain non-functional. The EL4 murine T cell lymphoma line (TIB-39) was acquired from the American Type Culture Collection (ATCC) and maintained in complete RPMI (RPMI-1640, 10% FBS [26140079, Life Technologies], 1% penicillin/streptomycin [Life Technologies]). EL4 T cell transfections were performed using the Lonza 4D nucleofection system (program CM-120, buffer SF). EL4 cells were nucleofected with

544 expression vectors for WT Aiolos, Aiolos^{DBM}, or an empty vector control in conjunction with pGL3-
545 *Stat1* and an SV40-*Renilla* vector as a control for transfection efficiency. After 22-24 hours of
546 recovery, samples were harvested, and luciferase expression was analyzed using the Dual-
547 Luciferase Reporter Assay System (Promega) according to the manufacturer's instructions.
548 Abundance of overexpressed proteins was assessed via immunoblot using an antibody against
549 the V5 epitope tag (Thermo Fisher Scientific, cat. # R960-25).
550
551 **Chromatin Immunoprecipitation (ChIP)**
552 ChIP assays were performed as described previously (98). In brief, chromatin was harvested from
553 in vitro-generated T_H1-like cells treated with IFNγ. Chromatin was incubated with antibodies
554 against STAT1 (ThermoFisher, cat. # 10144-2-AP; 7 µg per IP) or an IgG control (Abcam, cat. #
555 ab6709; 7 µg per IP, matched to experimental antibody), and the precipitated DNA was analyzed
556 by qPCR with gene-specific primers (Supplemental Table 3). Samples were normalized to a total
557 input DNA control, and percent enrichment was divided by IgG values. The final value represents
558 the percent enrichment fold change relative to the IgG control.
559
560 **Software summary**
561 Data were collected using the following open-source or commercially available software
562 programs: BD FACSDiva (version 8.0.2), BioRad Image Lab (version 6.0.1, build 34), BioRad
563 CFX Manager (version 3.1). Analyses and/or manuscript preparation were conducted using BD
564 FlowJo (version 10.8.1), and open-source software, including tools available on Integrative
565 Genomics Viewer (versions 2.12.3 and 2.18.2), Morpheus
566 (https://software.broadinstitute.org/morpheus), VolcaNoseR
567 (https://huygens.science.uva.nl/VolcaNoseR/), and Galaxy (usegalaxy.org). BioRender
568 (https://biorender.com/) was used to create schematics and the graphical abstract under licenses
569 to Leonard, M. (2024) (Supplemental Table 4). All statistical analyses were performed using

GraphPad Prism software (version 10). Data preparation for this manuscript did not require the use of custom code or software.

Statistics and reproducibility

All statistical analyses were performed using GraphPad Prism software (version 10). The ROUT method (Q = 1%) was used for identifying outliers. For single comparisons, two-tailed unpaired Student's *t* test was performed. For multiple comparisons, one-way ANOVA with Tukey's multiple comparisons test was performed. Error bars indicate the standard error of the mean (SEM). The *p* values <0.05 were considered statistically significant.

Study approval

This study complies with all ethical regulations defined by the Institutional Animal Care and Use Committee (IACUC) and Institutional Biosafety Committee (IBC) of The Ohio State University in Columbus, OH (IACUC #: 2019A00000107-R1). Animals were housed in the University Laboratory Animal Resources (ULAR) Health Sciences complex at The Ohio State University in rodent barrier housing utilizing individually ventilated caging systems. All animals used in this study were humanely euthanized via CO_2 inhalation.

Data availability

Published RNA-seq (GSE203065) and ATAC-seq (GSE203064) data sets were analyzed and used in this study. The following publicly available ChIP-seq data were obtained from ChIP Atlas (https://chip-atlas.org/) for use in this study: STAT1 (GSM994528), STAT4 (GSM550303), T-bet (GSM836124), Aiolos (GSM5106065). Values for all data points in graphs are reported in the Supporting Data Values file.

Author Contributions

M.R.L. assisted with the design of the study, performed experiments, analyzed data, and wrote the manuscript. D.M.J., K.A.R., S.P., J.A.T., and R.T.W. assisted with experiments and data analysis. J.S.Y. provided reagents for influenza virus infection experiments. K.J.O. supervised the research, designed the study, analyzed data, and edited the manuscript.

Acknowledgements

The authors would like to thank all current and former members of the Oestreich Laboratory, as well as colleagues in the Department of Microbial Infection and Immunity, for constructive feedback. The authors would also like to thank members of the Yount Laboratory for help with influenza virus preparation and Dr. Haitao Wen for providing OT-II animals. This work was supported by grants from the National Institutes of Health (R01AI134972 and R56AI127800 to K.J.O.) as well as funds from The Ohio State University College of Medicine and The Ohio State University Comprehensive Cancer Center (K.J.O.). M.R.L., S.P., and J.A.T. were supported by the National Institutes of Health T32 Interdisciplinary Program in Microbe-Host Biology (T32AI165391). S.P. was also supported by an American Heart Association Postdoctoral Fellowship (24POST1196412). J.A.T. was also supported by a National Institutes of Health Ruth L. Kirschstein National Research Service Award (1F30AI172189-01A1) and The Ohio State University Susan Huntington Dean's Distinguished University Fellowship. K.A.R. was supported by The Ohio State University College of Medicine Advancing Research in Infection and Immunity Fellowship Program.

References

1. O'Shea JJ, and Paul WE. Mechanisms underlying lineage commitment and plasticity of helper CD4+ T cells. *Science.* 2010;327(5969):1098-102.
2. Bonelli M, Shih HY, Hirahara K, Singelton K, Laurence A, Poholek A, et al. Helper T cell plasticity: impact of extrinsic and intrinsic signals on transcriptomes and epigenomes. *Curr Top Microbiol Immunol.* 2014;381:279-326.
3. Kanno Y, Vahedi G, Hirahara K, Singleton K, and O'Shea JJ. Transcriptional and epigenetic control of T helper cell specification: molecular mechanisms underlying commitment and plasticity. *Annu Rev Immunol.* 2012;30:707-31.
4. Christie D, and Zhu J. Transcriptional regulatory networks for CD4 T cell differentiation. *Curr Top Microbiol Immunol.* 2014;381:125-72.
5. Meitei HT, and Lal G. T cell receptor signaling in the differentiation and plasticity of CD4(+) T cells. *Cytokine Growth Factor Rev.* 2023;69:14-27.
6. Seif F, Khoshmirsafa M, Aazami H, Mohsenzadegan M, Sedighi G, and Bahar M. The role of JAK-STAT signaling pathway and its regulators in the fate of T helper cells. *Cell Commun Signal.* 2017;15(1):23.
7. Leonard WJ, and O'Shea JJ. Jaks and STATs: biological implications. *Annu Rev Immunol.* 1998;16:293-322.
8. Philips RL, Wang Y, Cheon H, Kanno Y, Gadina M, Sartorelli V, et al. The JAK-STAT pathway at 30: Much learned, much more to do. *Cell.* 2022;185(21):3857-76.
9. Hu X, Li J, Fu M, Zhao X, and Wang W. The JAK/STAT signaling pathway: from bench to clinic. *Signal Transduct Target Ther.* 2021;6(1):402.
10. Zhu J. T Helper Cell Differentiation, Heterogeneity, and Plasticity. *Cold Spring Harb Perspect Biol.* 2018;10(10).
11. Dobrzanski MJ. Expanding roles for CD4 T cells and their subpopulations in tumor immunity and therapy. *Front Oncol.* 2013;3:63.
12. Ylikoski E, Lund R, Kylaniemi M, Filen S, Kilpelainen M, Savolainen J, et al. IL-12 up-regulates T-bet independently of IFN-gamma in human CD4+ T cells. *Eur J Immunol.* 2005;35(11):3297-306.
13. Szabo SJ, Kim ST, Costa GL, Zhang X, Fathman CG, and Glimcher LH. A novel transcription factor, T-bet, directs Th1 lineage commitment. *Cell.* 2000;100(6):655-69.
14. Saravia J, Chapman NM, and Chi H. Helper T cell differentiation. *Cell Mol Immunol.* 2019;16(7):634-43.
15. Afkarian M, Sedy JR, Yang J, Jacobson NG, Cereb N, Yang SY, et al. T-bet is a STAT1-induced regulator of IL-12R expression in naive CD4+ T cells. *Nat Immunol.* 2002;3(6):549-57.
16. Read KA, Jones DM, Freud AG, and Oestreich KJ. Established and emergent roles for Ikaros transcription factors in lymphoid cell development and function. *Immunol Rev.* 2021;300(1):82-99.
17. Powell MD, Read KA, Sreekumar BK, and Oestreich KJ. Ikaros Zinc Finger Transcription Factors: Regulators of Cytokine Signaling Pathways and CD4(+) T Helper Cell Differentiation. *Front Immunol.* 2019;10:1299.
18. Read KA, Powell MD, Baker CE, Sreekumar BK, Ringel-Scaia VM, Bachus H, et al. Integrated STAT3 and Ikaros Zinc Finger Transcription Factor Activities Regulate Bcl-6 Expression in CD4(+) Th Cells. *J Immunol.* 2017;199(7):2377-87.
19. Yoshida T, and Georgopoulos K. Ikaros fingers on lymphocyte differentiation. *Int J Hematol.* 2014;100(3):220-9.
20. Heizmann B, Kastner P, and Chan S. The Ikaros family in lymphocyte development. *Curr Opin Immunol.* 2018;51:14-23.

21. John LB, and Ward AC. The Ikaros gene family: transcriptional regulators of hematopoiesis and immunity. *Mol Immunol.* 2011;48(9-10):1272-8.
22. Kim J, Sif S, Jones B, Jackson A, Koipally J, Heller E, et al. Ikaros DNA-binding proteins direct formation of chromatin remodeling complexes in lymphocytes. *Immunity.* 1999;10(3):345-55.
23. Yamashita M, Kuehn HS, Okuyama K, Okada S, Inoue Y, Mitsuiki N, et al. A variant in human AIOLOS impairs adaptive immunity by interfering with IKAROS. *Nat Immunol.* 2021;22(7):893-903.
24. Yamashita M, and Morio T. AIOLOS Variants Causing Immunodeficiency in Human and Mice. *Front Immunol.* 2022;13:866582.
25. Kuehn HS, Chang J, Yamashita M, Niemela JE, Zou C, Okuyama K, et al. T and B cell abnormalities, pneumocystis pneumonia, and chronic lymphocytic leukemia associated with an AIOLOS defect in patients. *J Exp Med.* 2021;218(12).
26. Kuehn HS, Sakovich IS, Niemela JE, Gil Silva AA, Stoddard JL, Polyakova EA, et al. Disease-associated AIOLOS variants lead to immune deficiency/dysregulation by haploinsufficiency and redefine AIOLOS functional domains. *J Clin Invest.* 2023.
27. Tuazon JA, Read KA, Sreekumar BK, Roettger JE, Yaeger MJ, Varikuti S, et al. Eos Promotes TH2 Differentiation by Interacting with and Propagating the Activity of STAT5. *J Immunol.* 2023;211(3):365-76.
28. Read KA, Jones DM, Pokhrel S, Hales EDS, Varkey A, Tuazon JA, et al. Aiolos represses CD4(+) T cell cytotoxic programming via reciprocal regulation of T(FH) transcription factors and IL-2 sensitivity. *Nat Commun.* 2023;14(1):1652.
29. Quintana FJ, Jin H, Burns EJ, Nadeau M, Yeste A, Kumar D, et al. Aiolos promotes TH17 differentiation by directly silencing Il2 expression. *Nat Immunol.* 2012;13(8):770-7.
30. Bromley SK, Mempel TR, and Luster AD. Orchestrating the orchestrators: chemokines in control of T cell traffic. *Nat Immunol.* 2008;9(9):970-80.
31. Kim CH, Rott L, Kunkel EJ, Genovese MC, Andrew DP, Wu L, et al. Rules of chemokine receptor association with T cell polarization in vivo. *J Clin Invest.* 2001;108(9):1331-9.
32. Charo IF, and Ransohoff RM. The many roles of chemokines and chemokine receptors in inflammation. *N Engl J Med.* 2006;354(6):610-21.
33. Groom JR, and Luster AD. CXCR3 in T cell function. *Exp Cell Res.* 2011;317(5):620-31.
34. Fowell DJ, and Kim M. The spatio-temporal control of effector T cell migration. *Nat Rev Immunol.* 2021;21(9):582-96.
35. Pontes Ferreira C, Moro Cariste L, Henrique Noronha I, Fernandes Durso D, Lannes-Vieira J, Ramalho Bortoluci K, et al. CXCR3 chemokine receptor contributes to specific CD8+ T cell activation by pDC during infection with intracellular pathogens. *PLoS Negl Trop Dis.* 2020;14(6):e0008414.
36. Groom JR, and Luster AD. CXCR3 ligands: redundant, collaborative and antagonistic functions. *Immunol Cell Biol.* 2011;89(2):207-15.
37. Melter M, Exeni A, Reinders ME, Fang JC, McMahon G, Ganz P, et al. Expression of the chemokine receptor CXCR3 and its ligand IP-10 during human cardiac allograft rejection. *Circulation.* 2001;104(21):2558-64.
38. Hancock WW, Lu B, Gao W, Csizmadia V, Faia K, King JA, et al. Requirement of the chemokine receptor CXCR3 for acute allograft rejection. *J Exp Med.* 2000;192(10):1515-20.
39. van Wanrooij EJ, de Jager SC, van Es T, de Vos P, Birch HL, Owen DA, et al. CXCR3 antagonist NBI-74330 attenuates atherosclerotic plaque formation in LDL receptor-deficient mice. *Arterioscler Thromb Vasc Biol.* 2008;28(2):251-7.
40. Steinmetz OM, Turner JE, Paust HJ, Lindner M, Peters A, Heiss K, et al. CXCR3 mediates renal Th1 and Th17 immune response in murine lupus nephritis. *J Immunol.* 2009;183(7):4693-704.

41. Muller M, Carter SL, Hofer MJ, Manders P, Getts DR, Getts MT, et al. CXCR3 signaling reduces the severity of experimental autoimmune encephalomyelitis by controlling the parenchymal distribution of effector and regulatory T cells in the central nervous system. *J Immunol.* 2007;179(5):2774-86.
42. Kuo PT, Zeng Z, Salim N, Mattarollo S, Wells JW, and Leggatt GR. The Role of CXCR3 and Its Chemokine Ligands in Skin Disease and Cancer. *Front Med (Lausanne).* 2018;5:271.
43. Liu L, Huang D, Matsui M, He TT, Hu T, Demartino J, et al. Severe disease, unaltered leukocyte migration, and reduced IFN-gamma production in CXCR3-/- mice with experimental autoimmune encephalomyelitis. *J Immunol.* 2006;176(7):4399-409.
44. Nakajima C, Mukai T, Yamaguchi N, Morimoto Y, Park WR, Iwasaki M, et al. Induction of the chemokine receptor CXCR3 on TCR-stimulated T cells: dependence on the release from persistent TCR-triggering and requirement for IFN-gamma stimulation. *Eur J Immunol.* 2002;32(6):1792-801.
45. Bouvier NM, and Lowen AC. Animal Models for Influenza Virus Pathogenesis and Transmission. *Viruses.* 2010;2(8):1530-63.
46. Kohlmeier JE, Cookenham T, Miller SC, Roberts AD, Christensen JP, Thomsen AR, et al. CXCR3 directs antigen-specific effector CD4+ T cell migration to the lung during parainfluenza virus infection. *J Immunol.* 2009;183(7):4378-84.
47. Zhao J, Zhao J, Mangalam AK, Channappanavar R, Fett C, Meyerholz DK, et al. Airway Memory CD4(+) T Cells Mediate Protective Immunity against Emerging Respiratory Coronaviruses. *Immunity.* 2016;44(6):1379-91.
48. Bettelli E, Sullivan B, Szabo SJ, Sobel RA, Glimcher LH, and Kuchroo VK. Loss of T-bet, but not STAT1, prevents the development of experimental autoimmune encephalomyelitis. *J Exp Med.* 2004;200(1):79-87.
49. Juedes AE, Rodrigo E, Togher L, Glimcher LH, and von Herrath MG. T-bet controls autoaggressive CD8 lymphocyte responses in type 1 diabetes. *J Exp Med.* 2004;199(8):1153-62.
50. Lord GM, Rao RM, Choe H, Sullivan BM, Lichtman AH, Luscinskas FW, et al. T-bet is required for optimal proinflammatory CD4+ T-cell trafficking. *Blood.* 2005;106(10):3432-9.
51. Beima KM, Miazgowicz MM, Lewis MD, Yan PS, Huang TH, and Weinmann AS. T-bet binding to newly identified target gene promoters is cell type-independent but results in variable context-dependent functional effects. *J Biol Chem.* 2006;281(17):11992-2000.
52. Barbi J, Oghumu S, Lezama-Davila CM, and Satoskar AR. IFN-gamma and STAT1 are required for efficient induction of CXC chemokine receptor 3 (CXCR3) on CD4+ but not CD8+ T cells. *Blood.* 2007;110(6):2215-6.
53. Koch MA, Tucker-Heard G, Perdue NR, Killebrew JR, Urdahl KB, and Campbell DJ. The transcription factor T-bet controls regulatory T cell homeostasis and function during type 1 inflammation. *Nat Immunol.* 2009;10(6):595-602.
54. Thieu VT, Yu Q, Chang HC, Yeh N, Nguyen ET, Sehra S, et al. Signal transducer and activator of transcription 4 is required for the transcription factor T-bet to promote T helper 1 cell-fate determination. *Immunity.* 2008;29(5):679-90.
55. Lewis MD, Miller SA, Miazgowicz MM, Beima KM, and Weinmann AS. T-bet's ability to regulate individual target genes requires the conserved T-box domain to recruit histone methyltransferase activity and a separate family member-specific transactivation domain. *Mol Cell Biol.* 2007;27(24):8510-21.
56. Vahedi G, Takahashi H, Nakayamada S, Sun HW, Sartorelli V, Kanno Y, et al. STATs shape the active enhancer landscape of T cell populations. *Cell.* 2012;151(5):981-93.

57. Wei L, Vahedi G, Sun HW, Watford WT, Takatori H, Ramos HL, et al. Discrete roles of STAT4 and STAT6 transcription factors in tuning epigenetic modifications and transcription during T helper cell differentiation. *Immunity.* 2010;32(6):840-51.
58. Nakayamada S, Kanno Y, Takahashi H, Jankovic D, Lu KT, Johnson TA, et al. Early Th1 cell differentiation is marked by a Tfh cell-like transition. *Immunity.* 2011;35(6):919-31.
59. Gil MP, Ploquin MJ, Watford WT, Lee SH, Kim K, Wang X, et al. Regulating type 1 IFN effects in CD8 T cells during viral infections: changing STAT4 and STAT1 expression for function. *Blood.* 2012;120(18):3718-28.
60. Liao W, Lin JX, Wang L, Li P, and Leonard WJ. Modulation of cytokine receptors by IL-2 broadly regulates differentiation into helper T cell lineages. *Nat Immunol.* 2011;12(6):551-9.
61. Sugimoto N, Nakahira M, Ahn HJ, Micallef M, Hamaoka T, Kurimoto M, et al. Differential requirements for JAK2 and TYK2 in T cell proliferation and IFN-gamma production induced by IL-12 alone or together with IL-18. *Eur J Immunol.* 2003;33(1):243-51.
62. Iwasaki M, Mukai T, Gao P, Park WR, Nakajima C, Tomura M, et al. A critical role for IL-12 in CCR5 induction on T cell receptor-triggered mouse CD4(+) and CD8(+) T cells. *Eur J Immunol.* 2001;31(8):2411-20.
63. Iwasaki M, Mukai T, Nakajima C, Yang YF, Gao P, Yamaguchi N, et al. A mandatory role for STAT4 in IL-12 induction of mouse T cell CCR5. *J Immunol.* 2001;167(12):6877-83.
64. Mikhak Z, Fleming CM, Medoff BD, Thomas SY, Tager AM, Campanella GS, et al. STAT1 in peripheral tissue differentially regulates homing of antigen-specific Th1 and Th2 cells. *J Immunol.* 2006;176(8):4959-67.
65. Mazzurana L, Forkel M, Rao A, Van Acker A, Kokkinou E, Ichiya T, et al. Suppression of Aiolos and Ikaros expression by lenalidomide reduces human ILC3-ILC1/NK cell transdifferentiation. *Eur J Immunol.* 2019;49(9):1344-55.
66. Bjorklund AK, Forkel M, Picelli S, Konya V, Theorell J, Friberg D, et al. The heterogeneity of human CD127(+) innate lymphoid cells revealed by single-cell RNA sequencing. *Nat Immunol.* 2016;17(4):451-60.
67. Collins PL, Cella M, Porter SI, Li S, Gurewitz GL, Hong HS, et al. Gene Regulatory Programs Conferring Phenotypic Identities to Human NK Cells. *Cell.* 2019;176(1-2):348-60 e12.
68. Fuchs A, Vermi W, Lee JS, Lonardi S, Gilfillan S, Newberry RD, et al. Intraepithelial type 1 innate lymphoid cells are a unique subset of IL-12- and IL-15-responsive IFN-gamma-producing cells. *Immunity.* 2013;38(4):769-81.
69. Holmes ML, Huntington ND, Thong RP, Brady J, Hayakawa Y, Andoniou CE, et al. Peripheral natural killer cell maturation depends on the transcription factor Aiolos. *EMBO J.* 2014;33(22):2721-34.
70. Gotthardt D, and Sexl V. STATs in NK-Cells: The Good, the Bad, and the Ugly. *Front Immunol.* 2016;7:694.
71. Lee CK, Rao DT, Gertner R, Gimeno R, Frey AB, and Levy DE. Distinct requirements for IFNs and STAT1 in NK cell function. *J Immunol.* 2000;165(7):3571-7.
72. Whitmire JK, Tan JT, and Whitton JL. Interferon-gamma acts directly on CD8+ T cells to increase their abundance during virus infection. *J Exp Med.* 2005;201(7):1053-9.
73. Krummel MF, Mahale JN, Uhl LFK, Hardison EA, Mujal AM, Mazet JM, et al. Paracrine costimulation of IFN-gamma signaling by integrins modulates CD8 T cell differentiation. *Proc Natl Acad Sci U S A.* 2018;115(45):11585-90.
74. Lazear HM, Schoggins JW, and Diamond MS. Shared and Distinct Functions of Type I and Type III Interferons. *Immunity.* 2019;50(4):907-23.
75. Liang S, Wei H, Sun R, and Tian Z. IFNalpha regulates NK cell cytotoxicity through STAT1 pathway. *Cytokine.* 2003;23(6):190-9.

76. Au-Yeung N, Mandhana R, and Horvath CM. Transcriptional regulation by STAT1 and STAT2 in the interferon JAK-STAT pathway. *JAKSTAT.* 2013;2(3):e23931.
77. Wei Y, Davenport TC, Collora JA, Ma HK, Pinto-Santini D, Lama J, et al. Single-cell epigenetic, transcriptional, and protein profiling of latent and active HIV-1 reservoir revealed that IKZF3 promotes HIV-1 persistence. *Immunity.* 2023;56(11):2584-601 e7.
78. Cabioglu N, Yazici MS, Arun B, Broglio KR, Hortobagyi GN, Price JE, et al. CCR7 and CXCR4 as novel biomarkers predicting axillary lymph node metastasis in T1 breast cancer. *Clin Cancer Res.* 2005;11(16):5686-93.
79. Muller A, Homey B, Soto H, Ge N, Catron D, Buchanan ME, et al. Involvement of chemokine receptors in breast cancer metastasis. *Nature.* 2001;410(6824):50-6.
80. Li X, Xu Z, Du W, Zhang Z, Wei Y, Wang H, et al. Aiolos promotes anchorage independence by silencing p66Shc transcription in cancer cells. *Cancer Cell.* 2014;25(5):575-89.
81. Terada LS, and Liu Z. Aiolos and Lymphocyte Mimicry in Lung Cancer. *Mol Cell Oncol.* 2014;1(1):e29912.
82. Hung JJ, Kao YS, Huang CH, and Hsu WH. Overexpression of Aiolos promotes epithelial-mesenchymal transition and cancer stem cell-like properties in lung cancer cells. *Sci Rep.* 2019;9(1):2991.
83. Chang J, Yamashita M, Padhi AK, Zhang KYJ, and Taniuchi I. Impaired tissue homing by the Ikzf3(N159S) variant is mediated by interfering with Ikaros function. *Front Immunol.* 2023;14:1239779.
84. O'Shea JJ, Holland SM, and Staudt LM. JAKs and STATs in immunity, immunodeficiency, and cancer. *N Engl J Med.* 2013;368(2):161-70.
85. Ivashkiv LB. IFNgamma: signalling, epigenetics and roles in immunity, metabolism, disease and cancer immunotherapy. *Nat Rev Immunol.* 2018;18(9):545-58.
86. Kulling PM, Olson KC, Hamele CE, Toro MF, Tan SF, Feith DJ, et al. Dysregulation of the IFN-gamma-STAT1 signaling pathway in a cell line model of large granular lymphocyte leukemia. *PLoS One.* 2018;13(2):e0193429.
87. Lu C, Ma H, Song L, Wang H, Wang L, Li S, et al. IFN-gammaR/STAT1 signaling in recipient hematopoietic antigen-presenting cells suppresses graft-versus-host disease. *J Clin Invest.* 2023;133(3).
88. Mitchell TJ, and John S. Signal transducer and activator of transcription (STAT) signalling and T-cell lymphomas. *Immunology.* 2005;114(3):301-12.
89. Lu G, Middleton RE, Sun H, Naniong M, Ott CJ, Mitsiades CS, et al. The myeloma drug lenalidomide promotes the cereblon-dependent destruction of Ikaros proteins. *Science.* 2014;343(6168):305-9.
90. Kronke J, Udeshi ND, Narla A, Grauman P, Hurst SN, McConkey M, et al. Lenalidomide causes selective degradation of IKZF1 and IKZF3 in multiple myeloma cells. *Science.* 2014;343(6168):301-5.
91. Kortum KM, Zhu YX, Shi CX, Jedlowski P, and Stewart AK. Cereblon binding molecules in multiple myeloma. *Blood Rev.* 2015;29(5):329-34.
92. Holstein SA, Hillengass J, and McCarthy PL. Next-Generation Drugs Targeting the Cereblon Ubiquitin Ligase. *J Clin Oncol.* 2018;36(20):2101-4.
93. Wang Z, Zhou G, Risu N, Fu J, Zou Y, Tang J, et al. Lenalidomide Enhances CAR-T Cell Activity Against Solid Tumor Cells. *Cell Transplant.* 2020;29:963689720920825.
94. Otahal P, Prukova D, Kral V, Fabry M, Vockova P, Lateckova L, et al. Lenalidomide enhances antitumor functions of chimeric antigen receptor modified T cells. *Oncoimmunology.* 2016;5(4):e1115940.
95. Yomogida K, Trsan T, Sudan R, Rodrigues PF, Ulezko Antonova A, Ingle H, et al. The transcription factor Aiolos restrains the activation of intestinal intraepithelial lymphocytes. *Nat Immunol.* 2023.

96. Barnden MJ, Allison J, Heath WR, and Carbone FR. Defective TCR expression in transgenic mice constructed using cDNA-based alpha- and beta-chain genes under the control of heterologous regulatory elements. *Immunol Cell Biol.* 1998;76(1):34-40.
97. Goedhart J, and Luijsterburg MS. VolcaNoseR is a web app for creating, exploring, labeling and sharing volcano plots. *Sci Rep.* 2020;10(1):20560.
98. McDonald PW, Read KA, Baker CE, Anderson AE, Powell MD, Ballesteros-Tato A, et al. IL-7 signalling represses Bcl-6 and the TFH gene program. *Nat Commun.* 2016;7:10285.

Figure Legends

Figure 1. CXCR3 expression is reduced on Aiolos-deficient T_H1 cells. A) Published RNA-seq data (GSE203065) from in vitro-generated WT and *Ikzf3*$^{-/-}$ T_H1 cells was assessed for differentially expressed genes (DEGs). A volcano plot displays gene expression changes at day 3. Genes are color-coded: no significant changes (gray), upregulated genes with >1.5-fold change with $p < 0.05$ (red), downregulated genes with >1.5-fold change with $p < 0.05$ (blue), and selected genes of interest (turquoise). **B)** Schematic of T_H1 cell culturing system. Naïve CD4$^+$ T cells were stimulated with α-CD3/CD28 under T_H1 polarizing conditions (IL-12, α-IL-4). On day 3, cells were harvested or removed from stimulation and placed into fresh T_H1 conditions with IL-2 for an additional 2 days. **C)** At day 3, transcript analysis was performed via qRT-PCR. Transcript was normalized to *Rps18* and presented as fold change compared to WT control (n = 10 biological replicates from 10 independent experiments, mean ± SEM; ****p<0.0001, two-tailed unpaired Student's t test). **D)** Representative flow cytometric analysis for CXCR3 on day 3 T_H1 cells. Data displayed as median fluorescence intensity (MFI) fold change compared to WT controls (n = 6 biological replicates from 6 independent experiments, mean ± SEM; ***p<0.001, two-tailed unpaired Student's t test). **E)** At day 5, transcript analysis was performed as in 'C' (n = 9 biological replicates from 9 independent experiments, mean ± SEM; ****p<0.0001, two-tailed unpaired Student's t test). Note: *Cxcr3* and *Ikzf3* transcript data presented here are the same as in Figure 5B. **F)** Representative flow cytometric analysis for CXCR3 on day 5 T_H1 cells. Data displayed as MFI fold change compared to WT controls (n = 5 biological replicates from 5 independent experiments, mean ± SEM; ****p<0.0001, two-tailed unpaired Student's t test).

Figure 2. CXCR3 expression is reduced on Aiolos-deficient CD4$^+$ T cells responding to IAV infection. A) Schematic of murine model of IAV infection. WT or *Ikzf3*$^{-/-}$ mice were infected intranasally with 30 PFU of IAV (A/PR/8/34; "PR8"). After 8 days, mediastinal lymph nodes (mLN)

and lungs were harvested and stained for flow cytometric analysis. Fluorochrome-labeled MHC II tetramers were used to identify IAV nucleoprotein (NP)-specific $CD4^+$ T cells. **B)** Representative flow cytometric analysis for CXCR3 expression in NP-specific $CD4^+$ T cells isolated from the mLN of WT or *Ikzf3*$^{-/-}$ mice. Data are compiled from 4 independent experiments and displayed as percent positive for CXCR3. **C)** Representative histogram overlay for CXCR3. Data are displayed as MFI fold change compared to WT controls (n = 16 for WT and n = 15 for *Ikzf3*$^{-/-}$, mean ± SEM; ****p<0.0001, two-tailed unpaired Student's t test).

Figure 3. CXCR3 expression is reduced on Aiolos-deficient $CD4^+$ T cells in a cell-intrinsic manner. A) Schematic of adoptive transfer system. Naïve $CD4^+$ T cells were harvested from the mLN of WT-OT-II or *Ikzf3*$^{-/-}$-OT-II mice. 500,000 cells/animal were adoptively transferred into $CD45.1^+$ recipients. Recipient mice were then infected with 40 PFU of $OVA_{323–339}$-expressing A/PR/8/34 ("PR8-OVA") influenza virus 24 hours post-transfer. 8 days post-infection, mLN was harvested and viable $CD45.2^+CD4^+CD62L^-CD44^+$ (antigen-specific, donor effector) cells were analyzed via flow cytometry. **B)** Representative flow cytometric analysis for CXCR3 expression in $CD45.2^+CD4^+CD62L^-CD44^+$ cells in the mLN. Data are compiled from 3 independent experiments and displayed as percent positive for CXCR3. **C)** Representative histogram overlay for CXCR3. Data are displayed as MFI fold change compared to WT-OT-II control cells (n = 13, mean ± SEM; ***p<0.001, ****p<0.0001, two-tailed unpaired Student's t test).

Figure 4. Aiolos-deficient T_H1 cells exhibit altered expression of components of IFNγ/STAT1 and IL-12/STAT4 signaling pathways. A) Publicly available Chromatin Immunoprecipitation sequencing (ChIP-seq) data for STAT1 (GSM994528), STAT4 (GSM550303), and T-bet (GSM836124) was examined at *Cxcr3*. Sequencing tracks were viewed using the Integrative Genomics Viewer (IGV). Regulatory regions of interest with transcription factor enrichment are indicated by the blue boxes. **B)** Published RNA-seq data (GSE203065)

from in vitro-generated WT and *Ikzf3*$^{-/-}$ T_H1 cells was analyzed for differentially expressed genes (DEGs). A heatmap of DEGs associated with IFNγ/STAT1 and IL-12/STAT4 signaling in T_H1 cells is shown, as well as additional genes involved in both pathways and T helper cell differentiation. Gene names color-coded in blue are downregulated in *Ikzf3*$^{-/-}$ T_H1 cells. Note: *Cxcr3* transcript data presented here are the same as in Supplemental Figure 3D. **C)** Schematic of proposed model in which Aiolos may regulate CXCR3 via impacts on components of the IFNγ/STAT1 and IL-12/STAT4 cytokine signaling pathways. The downward arrows in blue indicate genes that are downregulated in the absence of Aiolos.

Figure 5. IFNγ/STAT1 signaling, but not IL-12/STAT4, is diminished in IL-12-treated Aiolos-deficient T_H1 cells. A) Schematic of culturing system. Naïve $CD4^+$ T cells were stimulated with α-CD3/CD28 under T_H1 polarizing conditions (IL-12, α-IL-4). On day 3, cells were removed from stimulation and placed back into fresh T_H1 polarizing conditions (IL-12, α-IL-4) with IL-2 for an additional 2 days. **B)** At day 5, transcript analysis was performed via qRT-PCR. Transcript was normalized to *Rps18* and presented as fold change compared to WT control (n = 8-9 biological replicates from 8-9 independent experiments. Data are presented as mean ± SEM; ***p<0.001, ****p<0.0001, two-tailed unpaired Student's t test). Note: *Cxcr3* and *Ikzf3* transcript data presented here are the same as in Figure 1E. **C-D)** An immunoblot was performed to assess the relative abundance of the indicated proteins. β-actin serves as a loading control (n = 5-7 independent experiments, mean ± SEM; *p<0.05, ***p<0.001, ****p<0.0001, two-tailed unpaired Student's t test).

Figure 6. IFNγ/STAT1 signaling is compromised in IFNγ-treated Aiolos-deficient T_H1 cells. A) Schematic of culturing system. Naïve $CD4^+$ T cells were stimulated with α-CD3/CD28 and cultured under T_H1 polarizing conditions (IL-12, α-IL-4). On day 3, cells were removed from stimulation and given IFNγ, α-IL-4, and IL-2 for an additional 2 days. **B)** At day 5, transcript

analysis was performed via qRT-PCR. Transcript was normalized to *Rps18* and presented as fold change compared to WT control (n = 4 biological replicates from 4 independent experiments, mean ± SEM; **p<0.01, ***p<0.001, ****p<0.0001, two-tailed unpaired Student's t test). **C)** Representative flow cytometric analysis for CXCR3 on IFNγ-treated T_H1 cells at day 5. Data are displayed as MFI fold change compared to WT controls (n = 3 biological replicates from 3 independent experiments, mean ± SEM; **p<0.01, two-tailed unpaired Student's t test). **D)** An immunoblot was performed to assess the relative abundance of the indicated proteins. β-actin serves as a loading control (n = 4 independent experiments, mean ± SEM; *p<0.05, ***p<0.001, two-tailed unpaired Student's t test). **E)** ChIP assays were performed to assess STAT1 association with *Cxcr3* in WT and *Ikzf3*$^{-/-}$ T_H1 cells. Publicly available ChIP-seq data for STAT1 (GSM994528) was examined to identify potential regions of STAT1 enrichment. Sequencing tracks were viewed using IGV and regulatory regions of interest are indicated by blue boxes. Approximate ChIP primer locations at the *Cxcr3* promoter ("prom.") and 3' enhancer ("enhc.") are indicated with gray arrows. **F)** The indicated regions were analyzed for STAT1 enrichment. Data were normalized to total input. Percent enrichment relative to input was divided by IgG, and data are presented as fold change relative to IgG. (n = 4 biological replicates from 4 independent experiments, mean ± SEM; **p<0.01, ***p<0.001, one-way ANOVA with Tukey's multiple comparisons test).

Figure 7. IFNγ/STAT1 signaling induces Aiolos expression. A) Schematic of culturing system. WT naïve $CD4^+$ T cells were stimulated with α-CD3/CD28 under T_H1 polarizing conditions (IL-12, α-IL-4). Some cells were also treated with α-IFNγ to inhibit IFNγ/STAT1 signaling. **B)** At day 3, transcript analysis was performed via qRT-PCR. Transcript was normalized to *Rps18* and presented as fold change compared to WT control (n = 4 biological replicates from 4 independent experiments, mean ± SEM; **p<0.01, ****p<0.0001, two-tailed unpaired Student's t test). **C)** Representative flow cytometric analysis at day 3 for CXCR3 expression on WT T_H1 cells treated

with or without α-IFNγ. Data are displayed as percent positive for CXCR3 (n = 3 biological replicates from 3 independent experiments, mean ± SEM; *p<0.05, two-tailed unpaired Student's t test). **D)** An immunoblot was performed to assess the relative abundance of the indicated proteins. β-actin serves as a loading control (n = 4 independent experiments, mean ± SEM; *p<0.05, **p<0.01, ****p<0.0001, two-tailed unpaired Student's t test). **E)** At day 3, transcript and flow cytometric analyses were performed for *Ikzf3* and Aiolos protein expression, respectively. Flow cytometric data are displayed as MFI fold change compared to WT controls (n = 3 biological replicates from 3 independent experiments, mean ± SEM; **p<0.01, two-tailed unpaired Student's t test).

Figure 8. Aiolos and STAT1 engage in reciprocal regulation. A) Publicly available ATAC-seq data (GSE203064) from WT and *Ikzf3*$^{-/-}$ T_H1 cells was assessed for alterations in chromatin accessibility at the *Stat1* promoter. Publicly available ChIP-seq data for Aiolos (GSM5106065) was examined at *Stat1*. Sequencing tracks were viewed using IGV. The *Stat1* promoter region of significant differential accessibility is indicated by a blue box (p_{adj} = 0.0302). A ~500 bp region encompassing the indicated Aiolos DNA binding motifs within the *Stat1* promoter was cloned into a reporter plasmid. **B)** Schematic depicting the zinc finger (ZF) domains of WT Aiolos and a DNA-binding mutant (Aiolos^{DBM}). **C)** EL4 T cells were transfected with a *Stat1* promoter-reporter and either WT Aiolos, Aiolos^{DBM}, or empty vector control. Cells were also transfected with SV40-*Renilla* as a control for transduction efficiency. Luciferase promoter-reporter values were normalized to *Renilla* control and presented relative to the empty vector control. Aiolos was assessed via immunoblot with an antibody for the V5 epitope tag. β-actin serves as a loading control. Data are representative of 3 independent experiments (n = 3, mean ± SEM; *p<0.05, one-way ANOVA with Tukey's multiple comparisons test). **D)** Publicly available ATAC-seq data (GSE203064) from T_H1 cells and ChIP-seq data for STAT1 (GSM994528) were viewed using IGV to identify regions of STAT1 enrichment (blue box) at *Ikzf3*. Approximate ChIP primer locations

are indicated with a gray arrow. **E)** The *Ikzf3* promoter ("prom.") and a negative control region ("neg. ctrl.") were analyzed for STAT1 enrichment via ChIP. Data were normalized to total input. Percent enrichment relative to input was divided by IgG, and data are presented as fold change relative to IgG. (*n* = 4 biological replicates from 4 independent experiments, mean ± SEM; **p*<0.05, ***p*<0.01, one-way ANOVA with Tukey's multiple comparisons test).

Supplemental Figure 1. Aiolos-deficient mice have reduced numbers of CD4$^+$ T cells in the lungs during IAV infection. WT or *Ikzf3*$^{-/-}$ mice were infected intranasally with 30 PFU of IAV (A/PR/8/34; "PR8"). After 8 days, mLN and lungs were harvested and stained for flow cytometric analysis. Fluorochrome-labeled MHC II tetramers were used to identify IAV nucleoprotein (NP)-specific CD4$^+$ T cells. **A-B)** NP-specific CD4$^+$ T cells were enumerated. Cell numbers were normalized to 1 x 10^6 total events. Numbers and percentages of NP-specific CD4$^+$ T cells in the mLN and lungs are displayed. Data from 4 independent experiments is shown (For cell numbers, *n* = 17 for WT and *n* = 15 for *Ikzf3*$^{-/-}$. For percentages, *n* = 14 for mLN and *n* = 15 for lungs. Data are presented as mean ± SEM; *****p*<0.0001, two-tailed unpaired Student's *t* test). **C-D)** Bulk CD4$^+$ T cells were enumerated. Cell numbers were normalized to 1 x 10^6 total events. Numbers and percentages of bulk CD4$^+$ T cells in the mLN and lungs are displayed. Representative data from 4 independent experiments shown (For cell numbers, *n* = 17 for WT and *n* = 15 for *Ikzf3*$^{-/-}$. For percentages, *n* = 15 for mLN and *n* = 14 for lungs. Data are presented as mean ± SEM; *****p*<0.0001, two-tailed unpaired Student's *t* test).

Supplemental Figure 2. Aiolos-deficient mice exhibit no change in T-bet expression but have decreased CXCR3 expression during IAV infection. WT or *Ikzf3*$^{-/-}$ mice were infected intranasally with 30 PFU of IAV (A/PR/8/34; "PR8"). After 8 days, mLN and spleen were harvested and stained for flow cytometric analysis. Fluorochrome-labeled MHC II tetramers were used to identify IAV nucleoprotein (NP)-specific CD4$^+$ T cells in the mLN. **A)** Representative flow

cytometric analysis for T-bet expression in NP-specific cells isolated from the mLN of WT or *Ikzf3*$^{-/-}$ mice. Data are compiled from 4 independent experiments and displayed as MFI fold change compared to WT controls (n = 16 for WT and n = 15 for *Ikzf3*$^{-/-}$, mean ± SEM; two-tailed unpaired Student's t test). **B-D)** Representative flow cytometric analyses for CXCR3 expression in bulk CD4$^+$ naïve (CD62L$^+$CD44$^-$), central memory (CD62L$^+$CD44$^+$), and effector (CD62L$^-$CD44$^+$) T cell populations isolated from the spleens of WT or *Ikzf3*$^{-/-}$ mice. Data are compiled from 4 independent experiments and displayed as MFI fold change compared to WT controls (n = 17 for WT and n = 15 for *Ikzf3*$^{-/-}$, mean ± SEM; *p<0.05, ****p<0.0001, two-tailed unpaired Student's t test).

Supplemental Figure 3. CD4$^+$ T cells display altered migratory programs in the absence of Aiolos. Naïve CD4$^+$ T cells were harvested from the mLN and lungs of WT-OT-II or *Ikzf3*$^{-/-}$-OT-II mice. 500,000 cells/animal were adoptively transferred into CD45.1$^+$ recipients. Recipient mice were then infected with 40 PFU of $OVA_{323–339}$-expressing A/PR/8/34 ("PR8-OVA") influenza virus 24 hours post-transfer. 8 days post-infection, mLN and lungs were harvested and viable CD45.2$^+$CD4$^+$CD62L$^-$CD44$^+$ (antigen-specific, donor effector) cells were analyzed via flow cytometry. **A)** Representative flow cytometric analysis for T-bet expression in CD45.2$^+$CD4$^+$CD62L$^-$CD44$^+$ cells in the mLN. Data are compiled from 3 independent experiments and displayed as MFI fold change compared to WT-OT-II control cells (n = 13, mean ± SEM; ***p<0.001, two-tailed unpaired Student's t test). **B-C)** Total CD45.2$^+$ cell numbers were enumerated. Cell numbers were normalized to 500,000 total events. Numbers and percentages of CD45.2$^+$ cells in the mLN and lungs are displayed. Data from 3 independent experiments is shown (For cell numbers, n = 14-15. For percentages, n = 13-15. Data are presented as mean ± SEM; **p<0.01, two-tailed unpaired Student's t test). **D)** Published RNA-seq data (GSE203065) from in vitro-generated WT and *Ikzf3*$^{-/-}$ T_H1 cells was analyzed for differentially expressed genes (DEGs). A heatmap of DEGs associated with cell migration in T_H1 cells is shown. Gene names color-coded in blue are downregulated in *Ikzf3*$^{-/-}$ T_H1 cells. Gene names color-coded in red are

upregulated in *Ikzf3*$^{-/-}$ T_H1 cells. Note: *Cxcr3* transcript data presented here is the same as in Figure 4B. RTK; receptor tyrosine kinase. GEF; guanine nucleotide exchange factor.

Supplemental Figure 4. IFNγ/STAT1 and IL-12/STAT4 pathways are altered in Aiolos-deficient T_H1 cells. Naïve CD4$^+$ T cells were harvested from WT and *Ikzf3*$^{-/-}$ mice and stimulated with α-CD3/CD28 under T_H1 polarizing conditions (IL-12, α-IL-4). On day 3, cells were removed from stimulation and given either 1.) IL-12, α-IL-4, and IL-2 or 2.) IFNγ, α-IL-4, and IL-2 for an additional 2 days prior to harvest. **A)** At day 5, transcript analysis was performed on IL-12-treated T_H1 cells via qRT-PCR. Transcript was normalized to *Rps18* and presented as fold change compared to WT control (n = 4-8 biological replicates from 4-8 independent experiments. Data are presented as mean ± SEM; ***p<0.001, ****p<0.0001, two-tailed unpaired Student's t test). **B)** At day 5, RNA was isolated from IFNγ-treated T_H1 cells, and transcript analysis was performed as in 'A' (n = 4 biological replicates from 4 independent experiments, mean ± SEM; *p<0.05, ***p<0.001, two-tailed unpaired Student's t test). **C)** An immunoblot of IFNγ-treated T_H1 cells was performed to assess the relative abundance of the indicated proteins. β-actin serves as a loading control (n = 4 independent experiments, mean ± SEM; **p<0.01, two-tailed unpaired Student's t test).

Supplemental Figure 5. Representative flow cytometry gating strategy for mediastinal lymph node (mLN) and lungs in germline knockout IAV infection experiments. WT or *Ikzf3*$^{-/-}$ mice were infected intranasally with 30 PFU of IAV (A/PR/8/34; "PR8"). After 8 days, mLN and lungs were harvested and stained for flow cytometric analysis of CXCR3 and T-bet expression in IAV nucleoprotein (NP)-specific CD4$^+$ T cells. Fluorochrome-labeled MHC II tetramers were used to identify NP-specific cells in the mLN and lungs.

Supplemental Figure 6. Representative flow cytometry gating strategy for spleen in germline knockout IAV infection experiments. WT or *Ikzf3*$^{-/-}$ mice were infected intranasally with 30 PFU of IAV (A/PR/8/34; "PR8"). After 8 days, spleen was harvested and stained for flow cytometric analysis of CXCR3 expression in bulk CD4^{+} naïve (CD62L^{+}CD44^{-}), central memory (CD62L^{+}CD44^{+}), and effector (CD62L^{-}CD44^{+}) T cell populations.

Supplemental Figure 7. Representative flow cytometry gating strategy for adoptive transfer experiments. Naïve CD4^{+} T cells were harvested from the mLN of WT-OT-II or *Ikzf3*$^{-/-}$-OT-II mice. 500,000 cells/animal were adoptively transferred into CD45.1^{+} recipients. Recipient mice were then infected with 40 PFU of $OVA_{323–339}$-expressing A/PR/8/34 ("PR8-OVA") influenza virus 24 hours post transfer. 8 days post-infection, mLN was harvested and viable CD45.2^{+}CD4^{+} CD62L^{-} CD44^{+} (antigen-specific, donor effector) cells were analyzed via flow cytometry for CXCR3 and T-bet expression.

Main Figures

Figure 1

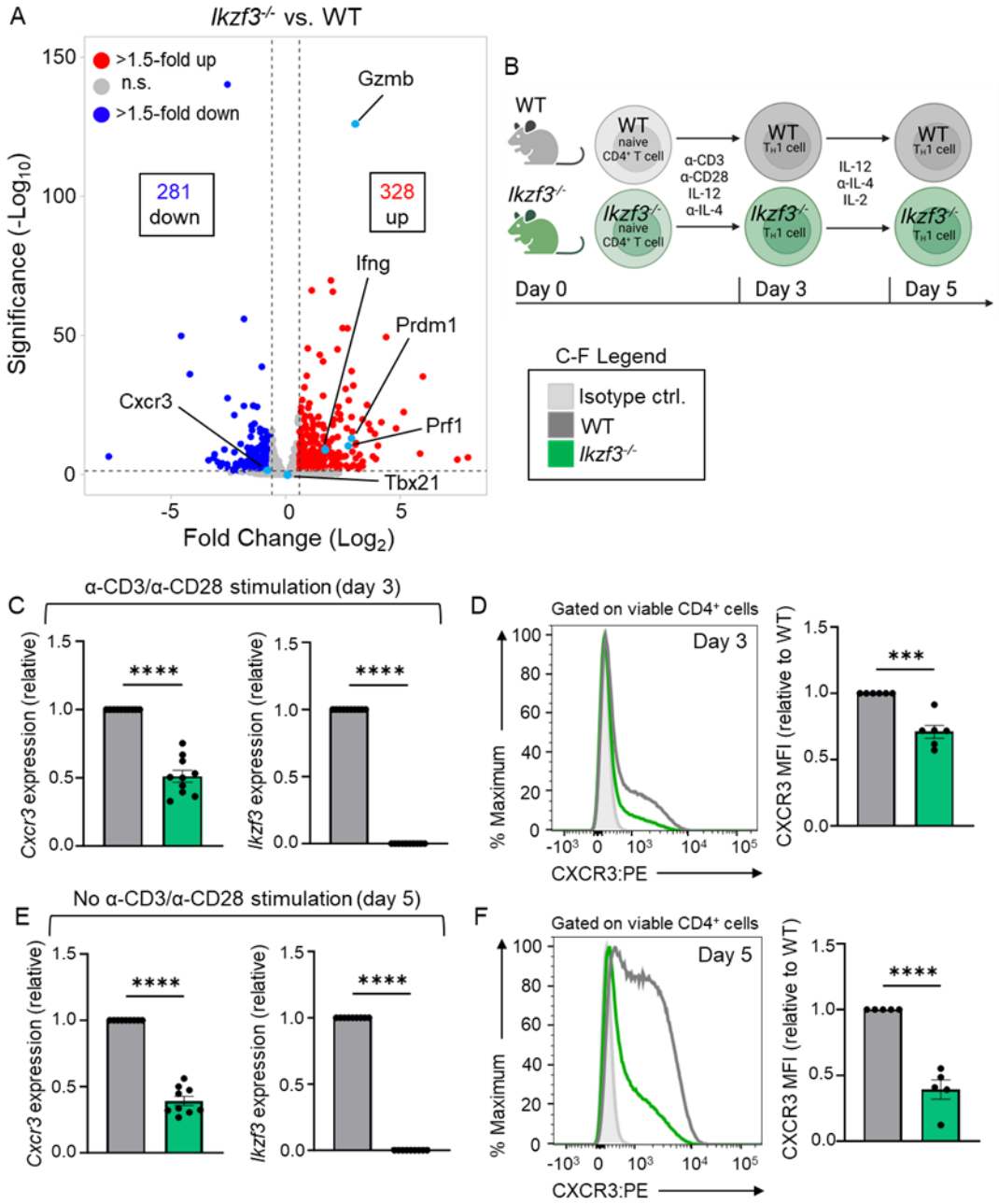

Figure 2

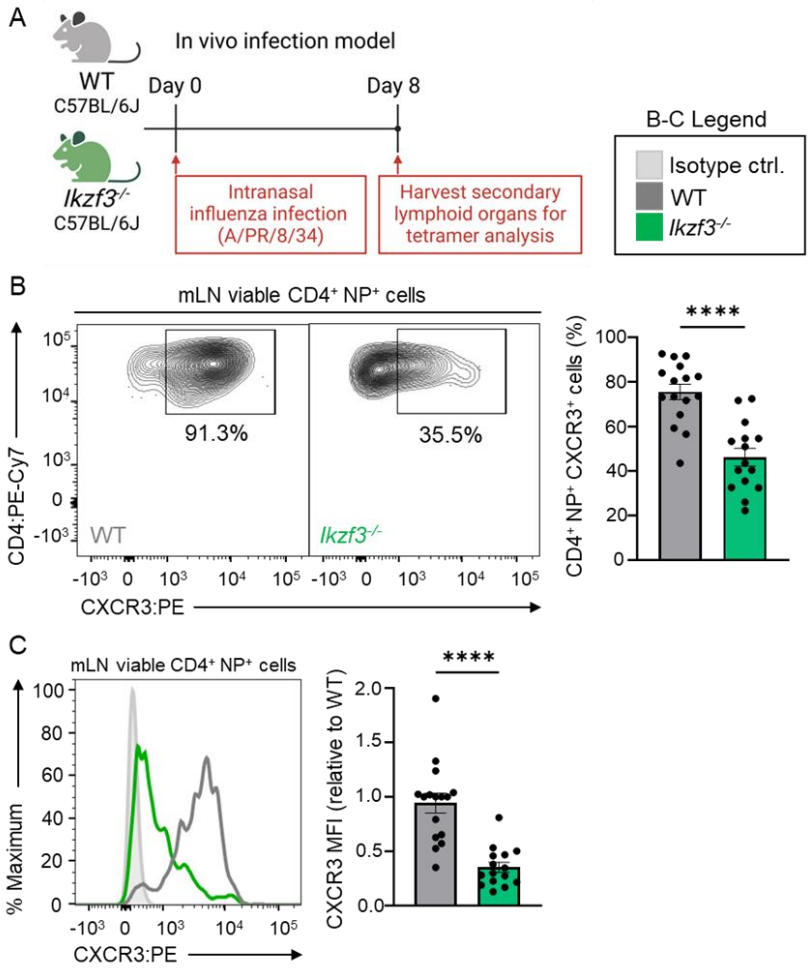
A
In vivo infection model
WT
C57BL/6J
Day 0
Day 8
Ikzf3-/-
C57BL/6J
Intranasal influenza infection (A/PR/8/34)
Harvest secondary lymphoid organs for tetramer analysis
B-C Legend
Isotype ctrl.
WT
Ikzf3-/-
B
mLN viable CD4+ NP+ cells
91.3%
35.5%
WT
Ikzf3-/-
CD4:PE-Cy7
CXCR3:PE
CD4+ NP+ CXCR3+ cells (%)
****
C
mLN viable CD4+ NP+ cells
% Maximum
CXCR3:PE
CXCR3 MFI (relative to WT)
****

Figure 3

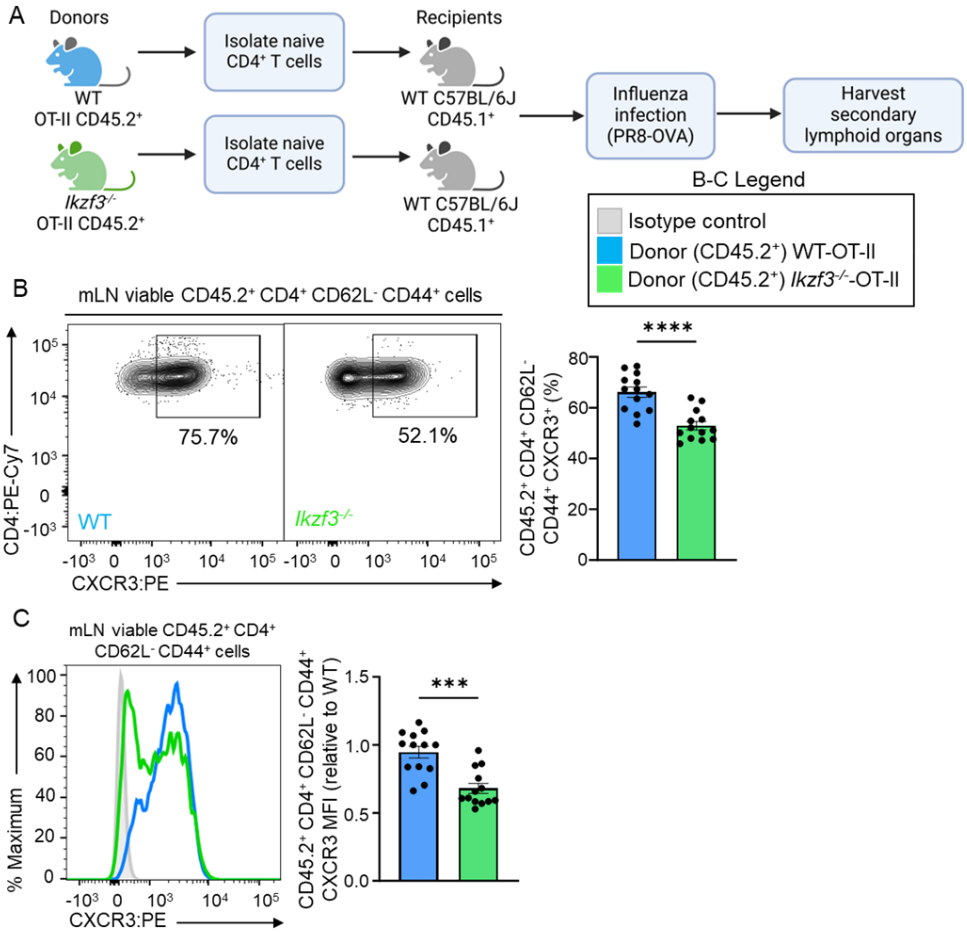
A
Donors
WT
OT-II CD45.2+
Ikzf3-/-
OT-II CD45.2+
Isolate naive CD4+ T cells
Isolate naive CD4+ T cells
Recipients
WT C57BL/6J CD45.1+
WT C57BL/6J CD45.1+
Influenza infection (PR8-OVA)
Harvest secondary lymphoid organs
B-C Legend
Isotype control
Donor (CD45.2+) WT-OT-II
Donor (CD45.2+) Ikzf3-/--OT-II
B
mLN viable CD45.2+ CD4+ CD62L- CD44+ cells
CD4:PE-Cy7
CXCR3:PE
75.7%
52.1%
WT
Ikzf3-/-
****
CD45.2+ CD4+ CD62L- CD44+ CXCR3+ (%)
C
mLN viable CD45.2+ CD4+ CD62L- CD44+ cells
% Maximum
CXCR3:PE
***
CD45.2+ CD4+ CD62L- CD44+ CXCR3 MFI (relative to WT)

Figure 4

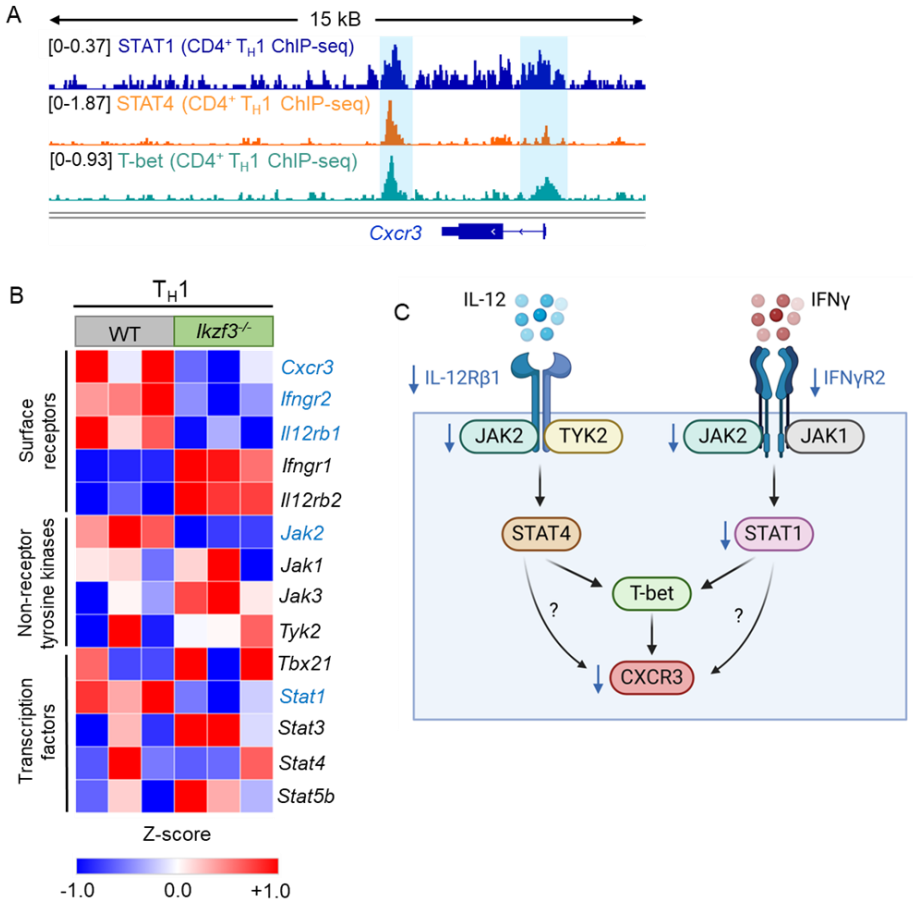
A
15 kB
[0-0.37] STAT1 (CD4+ TH1 ChIP-seq)
[0-1.87] STAT4 (CD4+ TH1 ChIP-seq)
[0-0.93] T-bet (CD4+ TH1 ChIP-seq)
Cxcr3
B
TH1
WT
Ikzf3-/-
Surface receptors
Non-receptor tyrosine kinases
Transcription factors
Cxcr3
Ifngr2
Il12rb1
Ifngr1
Il12rb2
Jak2
Jak1
Jak3
Tyk2
Tbx21
Stat1
Stat3
Stat4
Stat5b
Z-score
-1.0
0.0
+1.0
C
IL-12
IFNγ
IL-12Rβ1
IFNγR2
JAK2
TYK2
JAK2
JAK1
STAT4
STAT1
T-bet
?
?
CXCR3

Figure 5

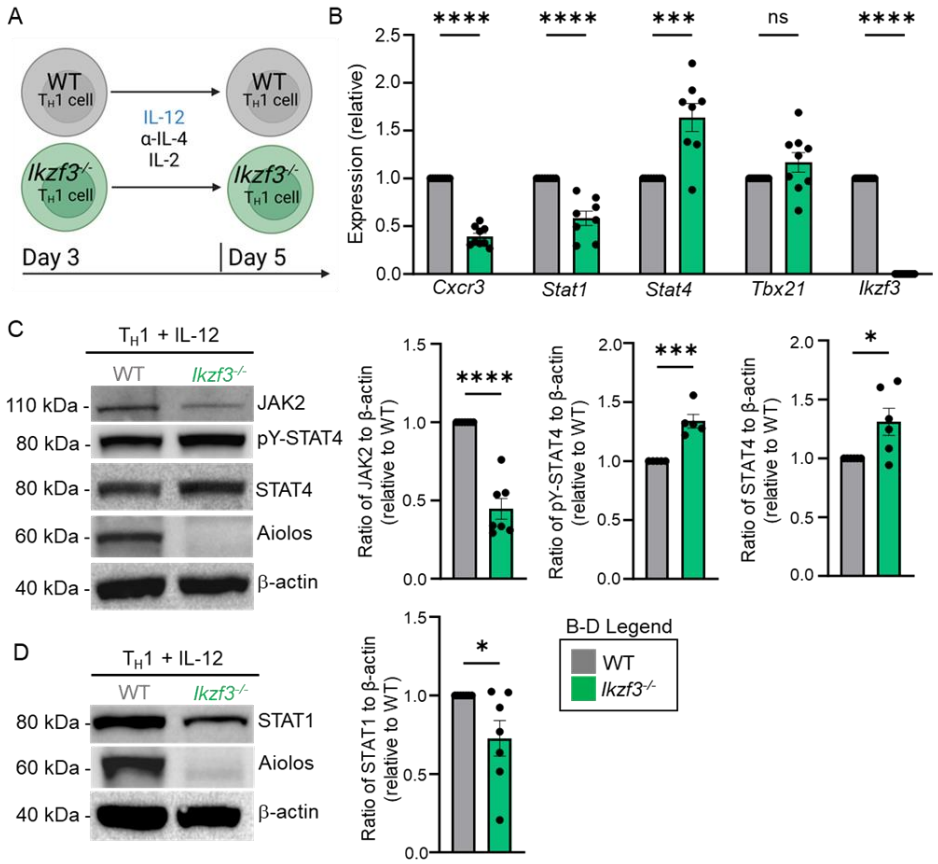
A
WT
TH1 cell
IL-12
α-IL-4
IL-2
Ikzf3-/-
TH1 cell
Day 3
Day 5
B
Expression (relative)
Cxcr3
Stat1
Stat4
Tbx21
Ikzf3
****
****
***
ns
****
C
TH1 + IL-12
WT
Ikzf3-/-
110 kDa
JAK2
80 kDa
pY-STAT4
80 kDa
STAT4
60 kDa
Aiolos
40 kDa
β-actin
Ratio of JAK2 to β-actin (relative to WT)
Ratio of pY-STAT4 to β-actin (relative to WT)
Ratio of STAT4 to β-actin (relative to WT)
D
TH1 + IL-12
WT
Ikzf3-/-
80 kDa
STAT1
60 kDa
Aiolos
40 kDa
β-actin
Ratio of STAT1 to β-actin (relative to WT)
B-D Legend
WT
Ikzf3-/-

Figure 6

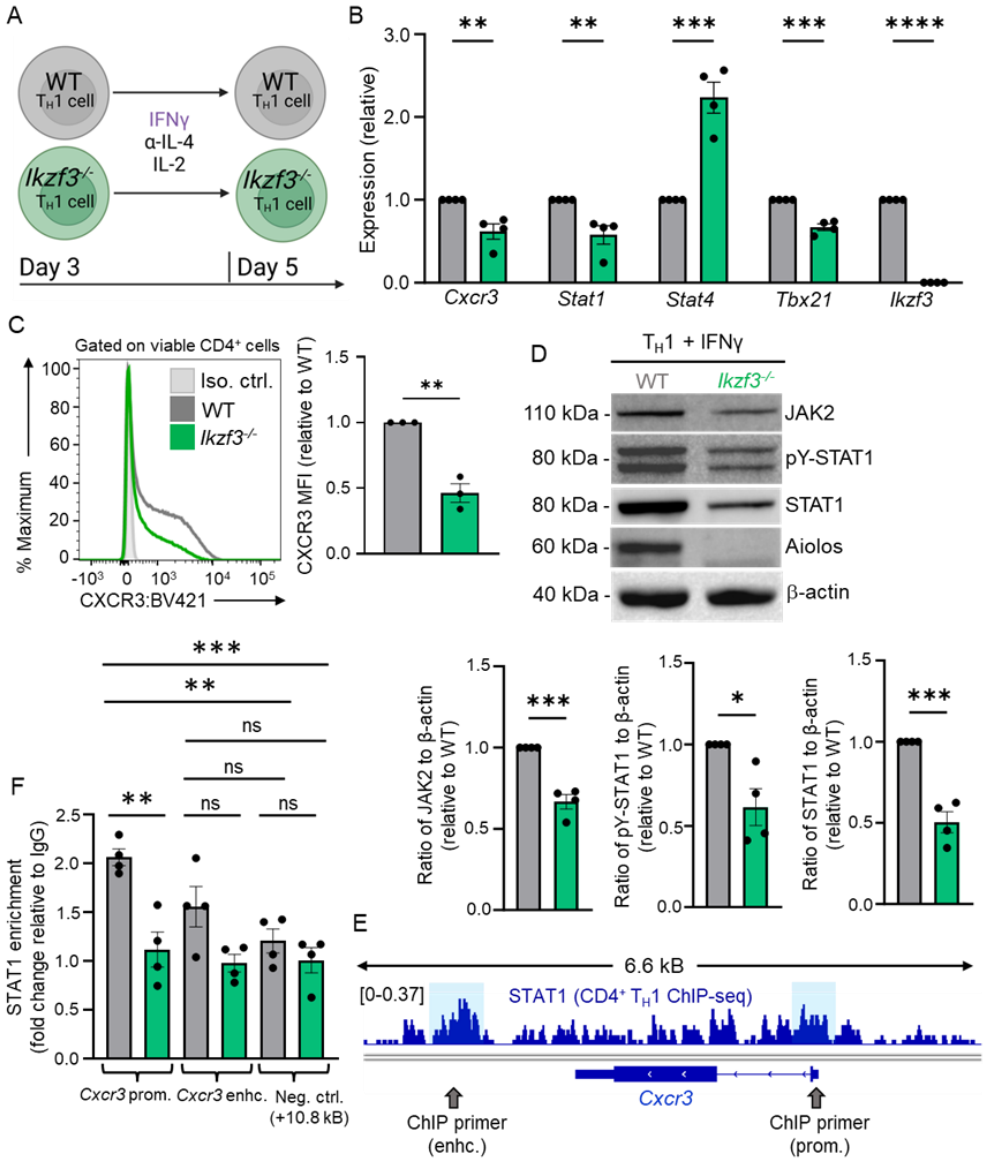
A
WT TH1 cell
WT TH1 cell
Ikzf3-/- TH1 cell
Ikzf3-/- TH1 cell
IFNγ
α-IL-4
IL-2
Day 3
Day 5
B
Expression (relative)
Cxcr3
Stat1
Stat4
Tbx21
Ikzf3
C
Gated on viable CD4+ cells
Iso. ctrl.
WT
Ikzf3-/-
% Maximum
CXCR3:BV421
CXCR3 MFI (relative to WT)
D
TH1 + IFNγ
WT
Ikzf3-/-
110 kDa
80 kDa
80 kDa
60 kDa
40 kDa
JAK2
pY-STAT1
STAT1
Aiolos
β-actin
E
6.6 kB
[0-0.37]
STAT1 (CD4+ TH1 ChIP-seq)
Cxcr3
ChIP primer (enhc.)
ChIP primer (prom.)
F
STAT1 enrichment (fold change relative to IgG)
Cxcr3 prom.
Cxcr3 enhc.
Neg. ctrl. (+10.8 kB)
Ratio of JAK2 to β-actin (relative to WT)
Ratio of pY-STAT1 to β-actin (relative to WT)
Ratio of STAT1 to β-actin (relative to WT)

Figure 7

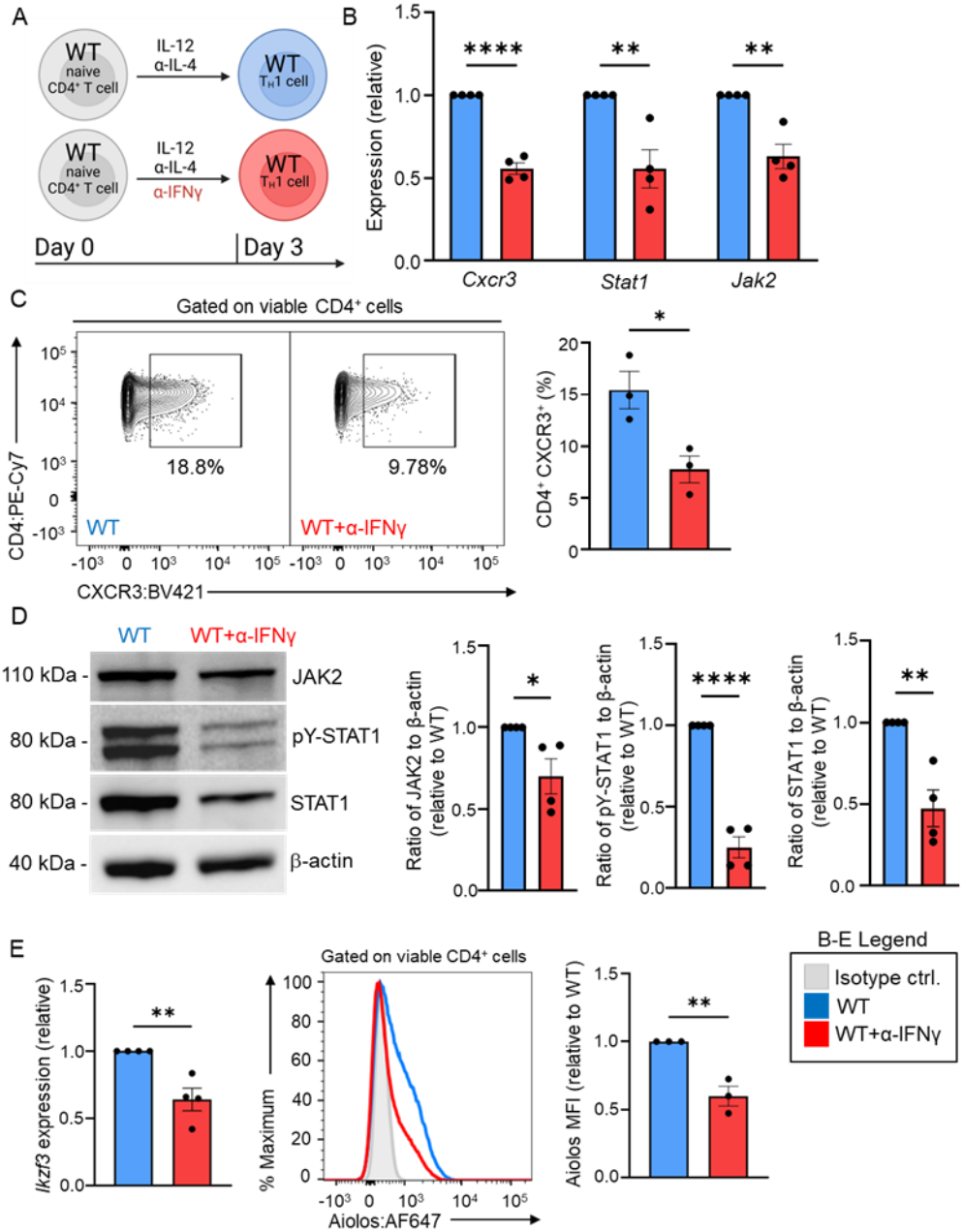
A
WT naive CD4+ T cell
IL-12
α-IL-4
WT TH1 cell
WT naive CD4+ T cell
IL-12
α-IL-4
α-IFNγ
WT TH1 cell
Day 0
Day 3
B
Expression (relative)
Cxcr3
Stat1
Jak2
C
Gated on viable CD4+ cells
CD4:PE-Cy7
CXCR3:BV421
18.8%
9.78%
WT
WT+α-IFNγ
CD4+ CXCR3+ (%)
D
WT
WT+α-IFNγ
110 kDa -
JAK2
80 kDa -
pY-STAT1
80 kDa -
STAT1
40 kDa -
β-actin
Ratio of JAK2 to β-actin (relative to WT)
Ratio of pY-STAT1 to β-actin (relative to WT)
Ratio of STAT1 to β-actin (relative to WT)
E
Ikzf3 expression (relative)
Gated on viable CD4+ cells
% Maximum
Aiolos:AF647
Aiolos MFI (relative to WT)
B-E Legend
Isotype ctrl.
WT
WT+α-IFNγ

Figure 8

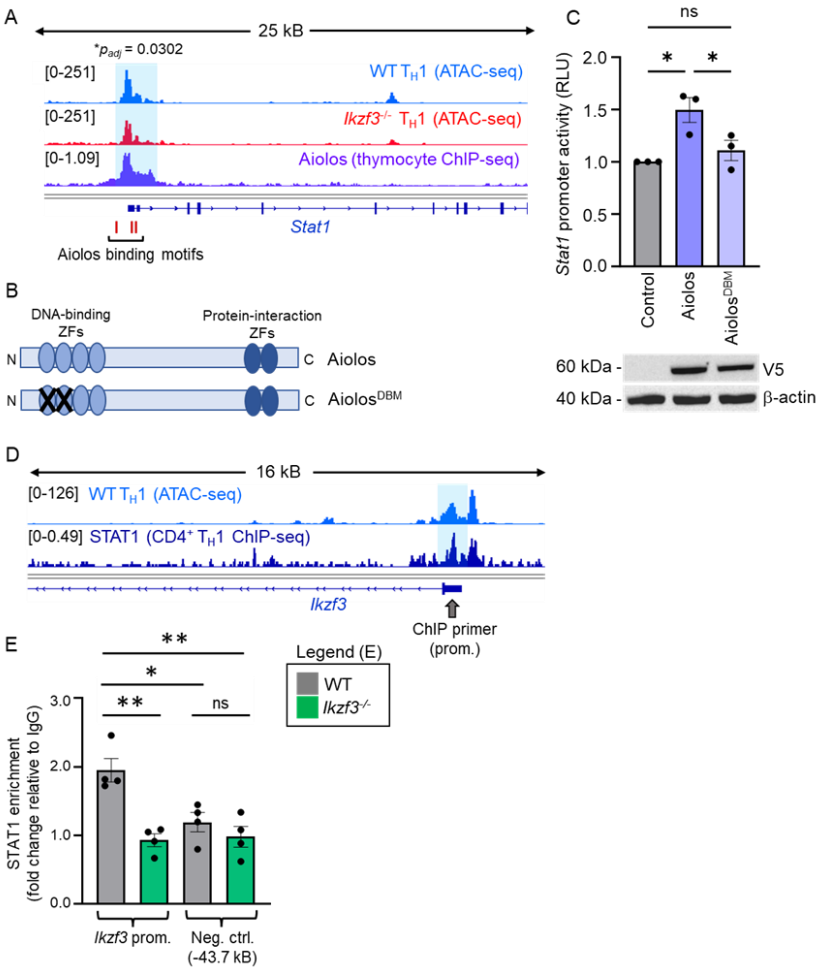
A
25 kB
*p_adj = 0.0302
[0-251]
WT T_H1 (ATAC-seq)
[0-251]
Ikzf3-/- T_H1 (ATAC-seq)
[0-1.09]
Aiolos (thymocyte ChIP-seq)
Stat1
I II
Aiolos binding motifs
B
DNA-binding ZFs
Protein-interaction ZFs
N
C
Aiolos
Aiolos^DBM
C
ns
*
*
Stat1 promoter activity (RLU)
2.0
1.5
1.0
0.5
0.0
Control
Aiolos
Aiolos^DBM
60 kDa -
40 kDa -
V5
β-actin
D
16 kB
[0-126] WT T_H1 (ATAC-seq)
[0-0.49] STAT1 (CD4+ T_H1 ChIP-seq)
Ikzf3
ChIP primer (prom.)
E
**
*
**
ns
Legend (E)
WT
Ikzf3-/-
STAT1 enrichment (fold change relative to IgG)
3.0
2.0
1.0
0.0
Ikzf3 prom.
Neg. ctrl. (-43.7 kB)

Supplemental Materials

Supplemental Figure 1

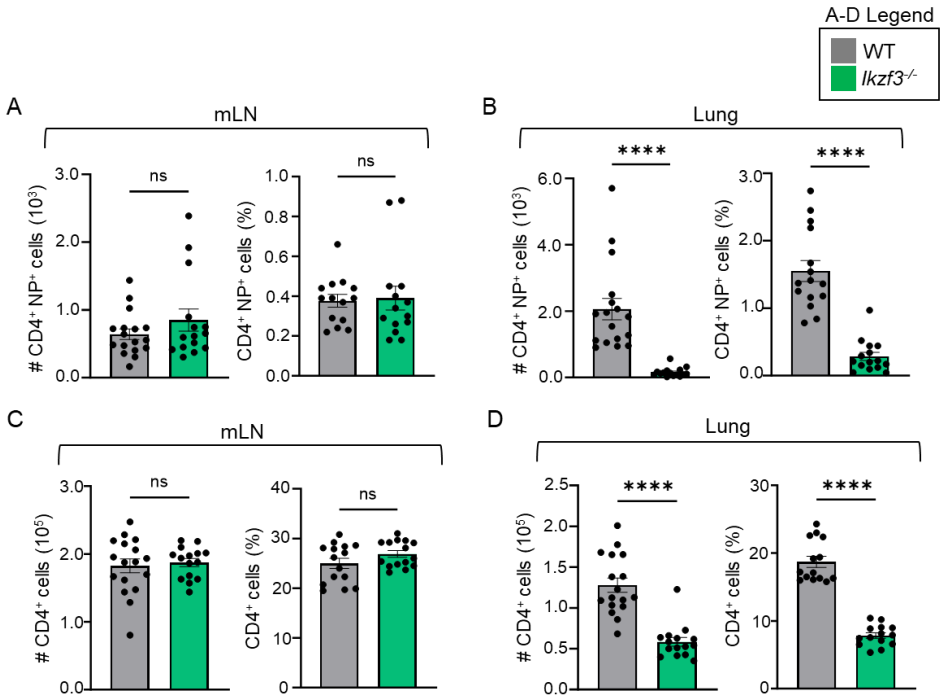

Supplemental Figure 2

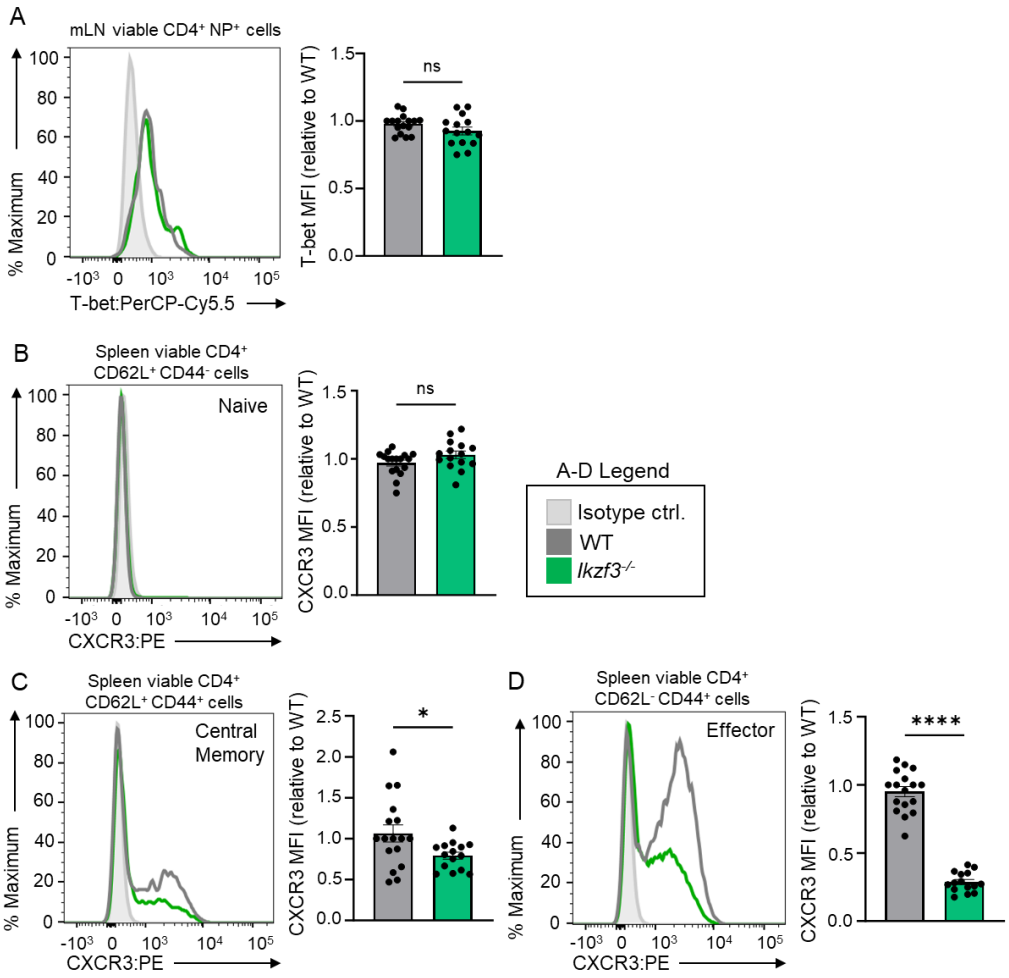

Supplemental Figure 3

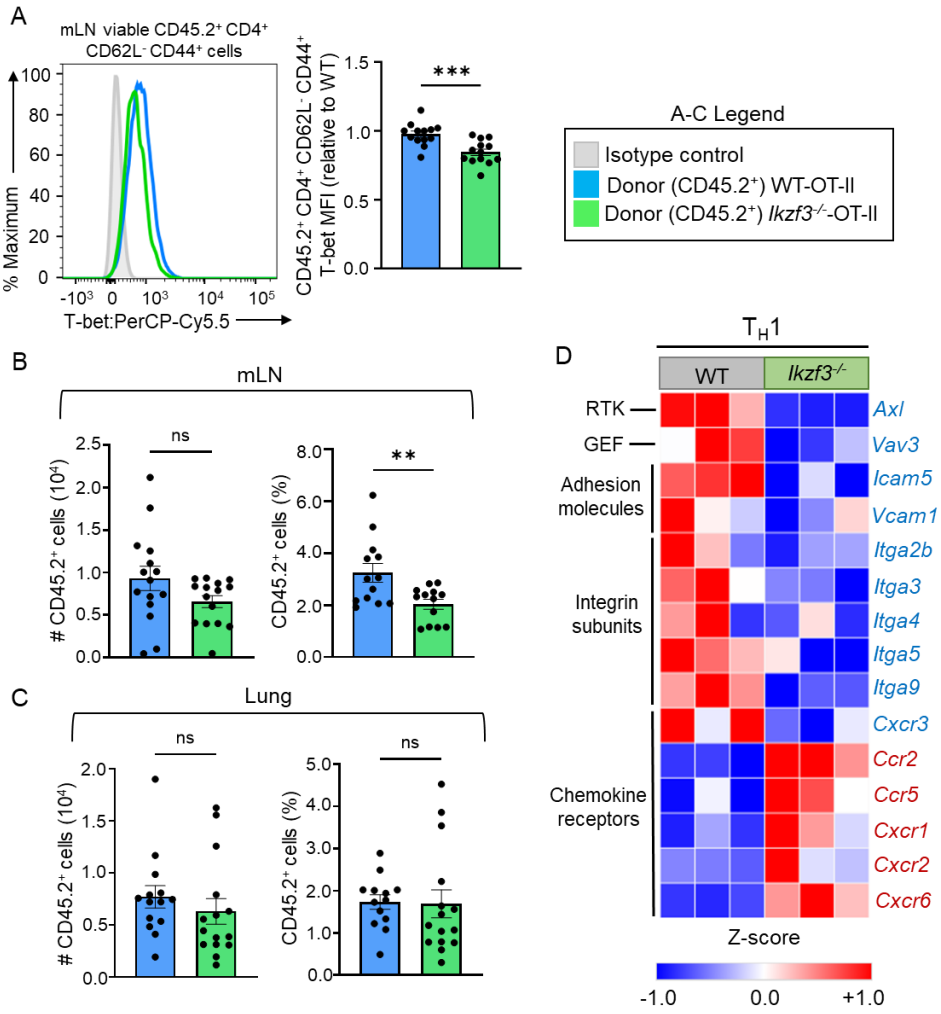

Supplemental Figure 4

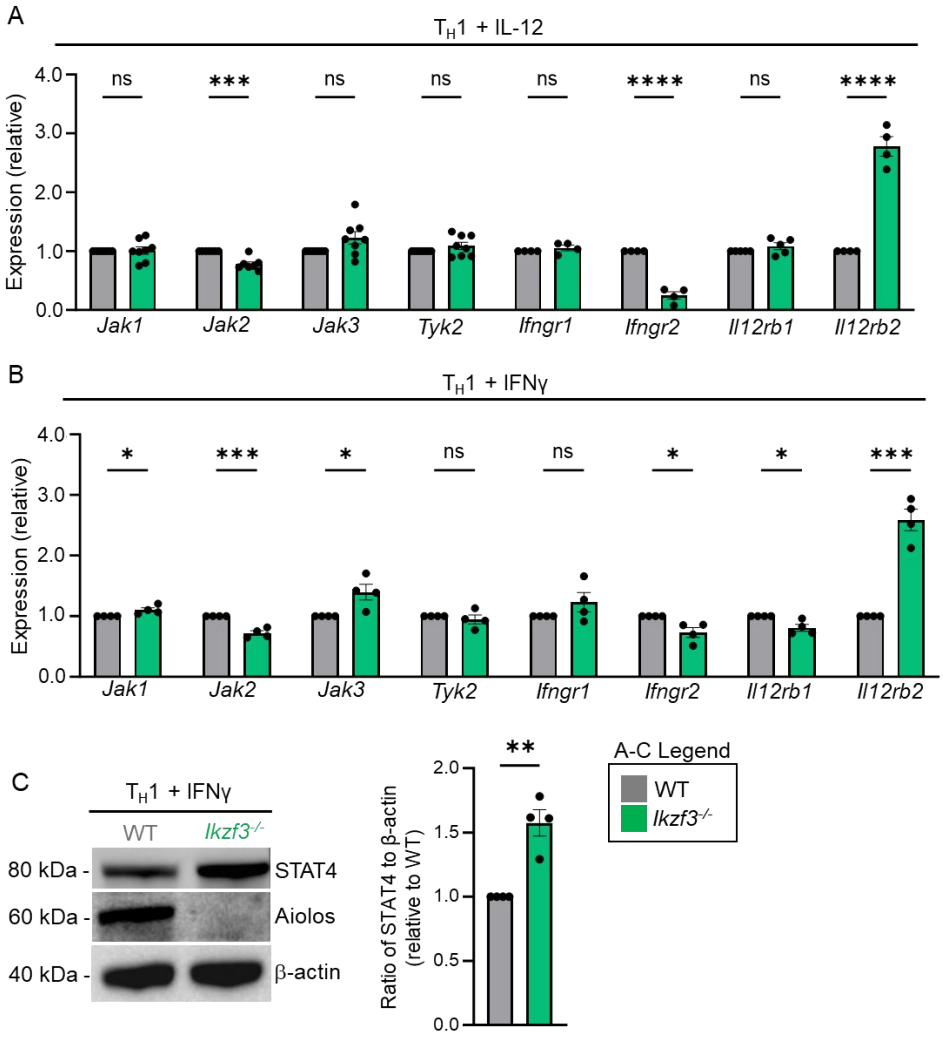

Supplemental Figure 5

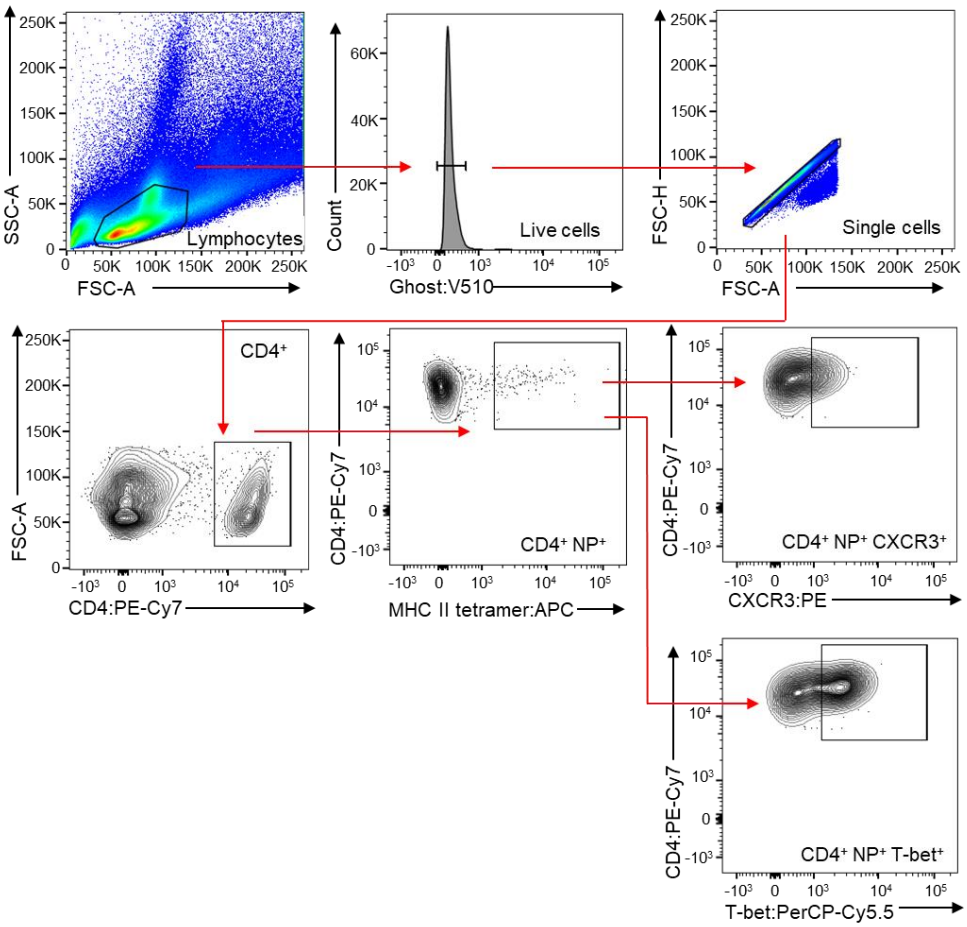

Supplemental Figure 6

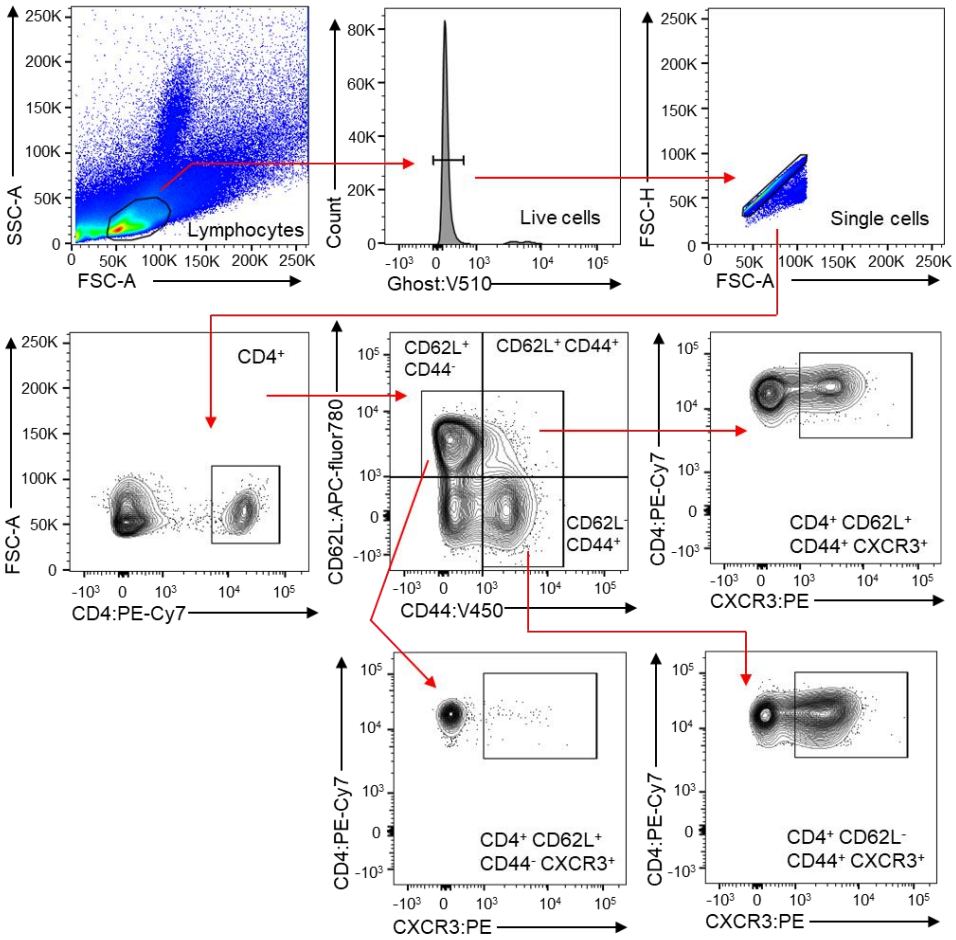

Supplemental Figure 7

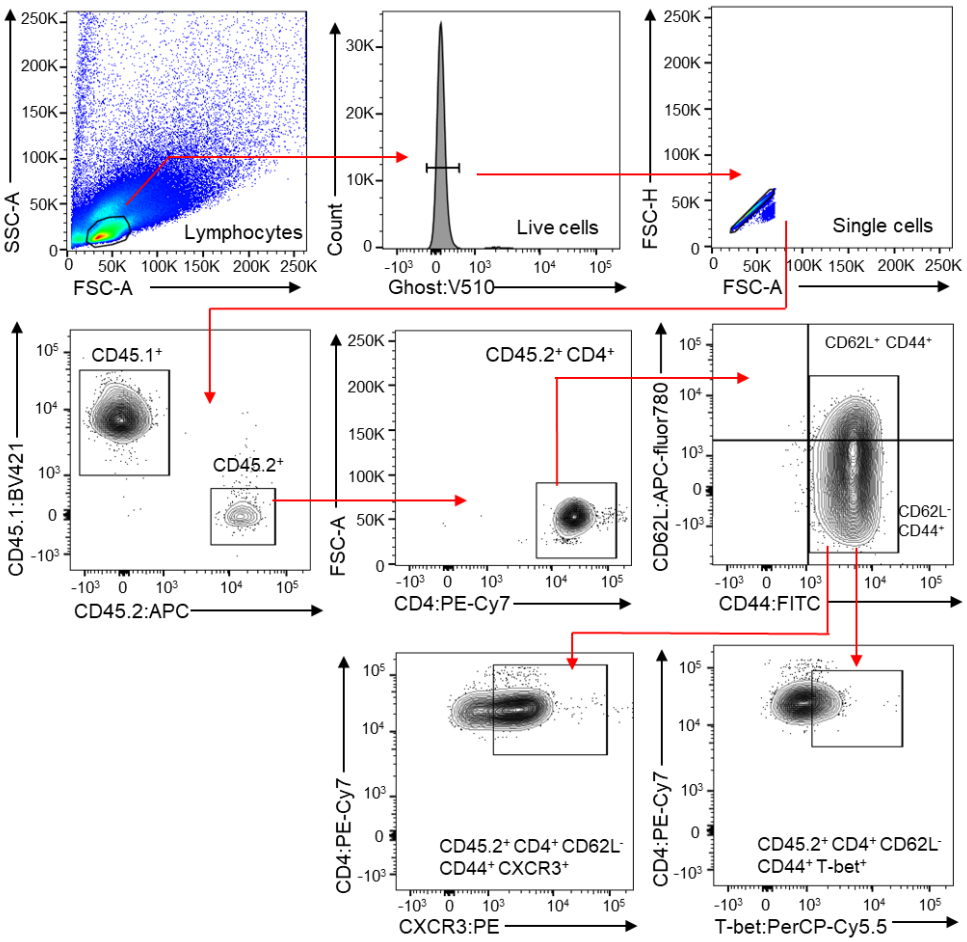

Supplemental Table 1. qRT-PCR primers

Gene (murine)	Forward (5'-3')	Reverse (5'-3')
Rps18	GGAGAACTCACGGAGGATGAG	CGCAGCTTGTTGTCTAGACCG
Ikzf3	CCGACTGTGGAGCTGAAAAGC	CCTGCATCTTCGTCTTCATTGG
Cxcr3	CCTTGAGGTTAGTGAACGTC	GCTGGCAGGAAGGTTCTGTC
Tbx21	GTGACTGCCTACCAGAACGC	AGGGGACACTCGTATCAACAG
Stat1	GGTACAACATGCTGGTGACAGAG	CTCCCAGCATGCTCAGCTGGTC
Stat4	CCAATGGGAGCCTCTCAGTGGAG	GCAACTCCTCTGTCACCATGTG
Jak1	GCTGAGGTGGAGCTGCACCGAC	GTCCATAGAGCCATGCAGGCTG
Jak2	GGAAACTTGGAGTGGCTAAGCAG	GTGGGTTCCCCGTTCTCCTGTC
Jak3	CCTGATCTGCGACTCCAGGC	GAGAATGTAGGTGCCTGGGAG
Tyk2	GGAGCGTCGCGTGCACATCCAC	GTGGCTGGAGTCAGCAGTCAAGC
Ifngr1	GTGTATGTGGAGCATAACCGGAG	CTGGAATCCAGTGTGGATACTGAG
Ifngr2	GAGCAATGTATCCTGTCACG	GTCAGGCCGAGCAGCAATGCG
Il12rb1	CACGACTCGGCTCCTCATGGAC	TCTCAACGCAGCCATCACC
Il12rb2	CTTGGACGGCATCAGTGTCTGC	GACCTGGTGAGGAGCCAGCAAC

Supplemental Table 2. Promoter-reporter primers

Gene (murine)	Forward (5'-3')	Reverse (5'-3')
***Stat1* prom.**	GATCGGTACCGCAGGCTTGGTTGACGTCAGTG	GATCGAGCTCAGGGCGTCCCGCCTCCTTCCGCCTC

Supplemental Table 3. ChIP qPCR primers

Gene (murine)	Forward (5'-3')	Reverse (5'-3')
***Cxcr3* prom.**	CAGGTCTCGTGCTGCCTGCTTCTC	CTGCGGAGGGCTGGTATAGATTACC
***Cxcr3* enhc.**	GGGAGAAAGTGACAGTGCAG	CAGACATTAGCATGAAGCCACC
***Cxcr3* ctrl.**	GCCTAGGGAAGATAGTTCCTC	GGTTGAAGCAGGGAGTGGTGG
***Ikzf3* prom.**	GACGTCTACTTGAGAAACACCGG	CACTGACAGTTCTCAAGACCGTC
***Ikzf3* ctrl.**	GTGCAGCTTCCCAATAAACCTGCC	GGAACTCACCATGTAGACCAGGCTG

Supplemental Table 4. BioRender Publication Licenses

Figure	Citation
Graphical abstract	Leonard, M. (2024) https://BioRender.com/i42i899
Figure 1B	Leonard, M. (2024) https://BioRender.com/v70c175
Figure 2A	Leonard, M. (2024) https://BioRender.com/p22p915
Figure 3A	Leonard, M. (2024) https://BioRender.com/h43w136
Figure 4C	Leonard, M. (2024) https://BioRender.com/b87z682
Figure 5A	Leonard, M. (2024) https://BioRender.com/i17z581
Figure 6A	Leonard, M. (2024) https://BioRender.com/u39m539
Figure 7A	Leonard, M. (2024) https://BioRender.com/r22y787